Università degli Studi di Ferrara

DOTTORATO DI RICERCA IN
SCIENZE DELL'INGEGNERIA

Ciclo XXX

Coordinatore: Prof. S. Trillo

Performance Evaluation in External Gear Pumps: Numerical and Experimental Methods

Settore Scientifico Disciplinare ING/IND 13

Dottorando	**Tutore**
Dott. Mattia Battarra	Prof. Emiliano Mucchi

Anni 2014/2017

Non ti preoccupare, quando ti sposi non te lo ricordi più.

Mio nonno

PREFACE

I graduated *cum laude* in Mechanical Engineering at the University of Ferrara in December, 2013. Just after the graduation, I have joined the research group leaded by Prof. G. Dalpiaz by taking part of the European Project COST TU1105 entitled *'NVH Analysis techniques for design and optimization of hybrid and electric vehicles'*. Within this framework, I spent three month at the Dynamic Research Group, Loughborough University, England, working in a research team constituted by three other junior researchers and two supervisors, Prof. S. Theodossiades and Prof. S. Walsh. During this experience abroad, my colleagues and I performed a Transfer and Operational Path Analysis on an electric vehicle provided by the PSA Group; results have been published in [1]:

[1] A. Diez-Ibarbia, M. Battarra, J. Palenzuela, G. Cervantes, S. Walsh, M. De-la Cruz, S. Theodossiades, and L. Gagliardini. “Comparison between transfer path analysis methods on an electric vehicle.” In: *Applied Acoustics* 118 (2017), pp. 83–101. DOI: `10.1016/j.apacoust.2016.11.015`.

Since I came back to the University of Ferrara, my research activity has been mainly focused on developing numerical models for simulating gear pumps in terms of dynamic behavior and efficiency, becoming the research topic of my PhD studies. Thanks to a valuable collaboration with ZF-TRW Automotive Italia s.r.l., I had the chance to pay particular attention on the possibility to evaluate a number of uncommon design solutions that are peculiar requirements in the field of high performance automotive applications. During the first year of my PhD, I developed a lumped parameter model to simulate efficiency and pressure ripple characteristics of tandem gear pumps [2], i.e. gear pumps with multiple parallel and coaxial stages; quality of the results have been supported by comparing them with experimental data. Later, the modeling approach has been improved, with the aim to evaluate the actual positioning of the gear center and therefore to determine the actual radial clearances. The development of such a model has started with the definition of a dedicated procedure for the calculation of the variable pressure loads applied to the gears [3, 4]; the procedure has been defined for both spur and helical gear pumps and compared with other methods described in the literature.

[2] M. Battarra, E. Mucchi, and G. Dalpiaz. "A model for the estimation of pressure ripple in tandem gear pumps." In: *ASME IDETC/CIE*. 2015, V010T11A018; 9 pages. DOI: `10.1115/DETC2015-46338`.

[3] M. Battarra and E. Mucchi. "A method for variable pressure load estimation in spur and helical gear pumps." In: *Mechanical Systems and Signal Processing* 76-77 (2016), pp. 265–282. DOI: `10.1016/j.ymssp.2016.02.020`.

[4] M. Battarra and E. Mucchi. "Evaluating time dependent pressure forces and torques in external gear machines by means of an analytical approach." In: *Internoise 2017*. Honk Kong, 2017, pp. 6737–6748.

During my second year, I spent 5 month at the GearLab, Ohio State University, Columbus (OH) - USA, under the supervision of Prof A. Kahraman. This experience abroad gave me the chance to deepen my studies on the dynamic behavior of gear pumps, which led me to develop a non-linear model to evaluate gear pump dynamics at the earliest stages of the design process, when a number of design parameters are still unknown and, therefore, high-accuracy models cannot be applied. Later, in my third year I extended the lumped parameter model previously developed to the simulation of gear pumps with non-unitary transmission ratio and validated the results by means of a dedicated experimental campaign. Within this context, I also had the chance to focus my studies on cavitation, which may take place in gear pumps working at high speed, producing tremendous effects on both the machine efficiency and reliability. Firstly, the phenomenon, rarely studied in the literature in correlation with gear pumps, has been experimentally characterized and later a dedicated modeling approach has been proposed.

Apart from my PhD research topic, I also had the chance to study the dynamics of other mechanical systems; in particular, I addressed the evaluation of the NVH behavior of linear vibratory feeders by proposing a minimal model to study the influence of the frames mechanism on the driveline of the feeder [5, 6].

[5] M. Buzzoni, M. Battarra, E. Mucchi, and G. Dalpiaz. "Noise and vibration improvements in vibratory feeders by analytical models and experimental analysis." In: *Internoise 2017*. Honk Kong, 2017, pp. 6749–6759.

[6] M. Buzzoni, M. Battarra, E. Mucchi, and G. Dalpiaz. “Motion analysis of a linear vibratory feeder : Dynamic modeling and experimental verification.” In: *Mechanism and Machine Theory* 114 (2017), pp. 98–110. DOI: `10.1016/j.mechmachtheory.2017.04.006`.

This brief summary regarding the work I carried out in the last three years leads me to express sincere gratitude to ZF-TRW Automotive Italia s.r.l. and its engineers for their active co-operation during the experimental studies. A special thank goes to my advisor, Prof. E. Mucchi, and to Prof. G. Dalpiaz and Eng. G. D’elia, for the help and the time they dedicated me throughout this experience.

Finally, I want to sincerely thank my office mates, who shared the PhD experience with me, and all the other guys that work in the research group.

CONTENTS

LIST OF FIGURES

LIST OF TABLES

NOMENCLATURE

Latin symbols

B	oil bulk's modulus
b	gear facewidth
$\mathbf{C}$	damping matrix
c	damping coefficient
C_d	discharge coefficient
F_m	mesh force
$\mathbf{F_p}$	pressure loads vector
F_p	pressure force
J	polar mass moment of inertia
$\mathbf{K}$	stiffness matrix
k_m	mesh stiffness
$\mathbf{M}$	mass matrix
m	mass
m_n	normal module
P	oil pressure
P_{in}	suction pressure
P_{sat}	saturation pressure
P_{trap}	oil pressure inside the trapped volume
P_{out}	delivery pressure
p_b	base pitch
Q	volumetric flowrate
Q^{in}	volumetric flowrate entering inside the control volume

Q_{inlet}	volumetric flowrate exchanged with the suction chamber
Q_m	volumetric flowrate exchanged between meshing pockets
Q^{out}	volumetric flowrate escaping from the control volume
Q_{outlet}	volumetric flowrate exchanged with the delivery chamber
r	base radius
r_{ext}	radius of the tip circle
r_o	radius of the pitch circle
r_{root}	radius of the root circle
T	torque
t	time
$\mathbf{T_d}$	friction torque vector
T_{oil}	oil temperature
T_{shaft}	torque required to work the pump
u	tangential velocity
V	volume of a generic tooth pocket
V_m	pump theoretical displacement
$\bar{x}_b$	half of the backlash clearance
$\bar{x}_r$	relative gear mesh displacement

Greek symbols

α	pressure angle
β	helix angle
ε	gearpair contact ratio
ζ	modal damping
η_{HM}	pump hydro-mechanical efficiency
η_V	pump volumetric efficiency
ϑ	nominal rotational angle

θ	rotational vibration around the nominal rotational angle
μ	oil dynamic viscosity
ω	angular speed
ρ	oil density
σ	cavitation number
τ	transmission ratio

Subscripts & superscripts

$(1), (2)$	denote driving and driven gear, respectively, in case of vectors or vector components
$1, 2$	denote driving and driven gear, respectively
i, j	denote isolated tooth pocket on the driving and driven gear, respectively
x, y, z	denote direction of application

1

INTRODUCTION

1.1 GEAR PUMPS IN MODERN AUTOMOTIVE AUXILIARY SYSTEMS

Gear pumps are nowadays considered as useful power providers for several applications, due to their features regarding the wide operating condition range, small dimensions, high reliability and reduced costs. They are commonly adopted as oil supplying components in various automotive subsystems such as automatic transmissions, steering systems and engine lubrication circuits. Depending on the application, these machines are required to perform opposite tasks: they are typically used to provide a high delivery flow rate with low pressure content in case of cooling and lubrication circuits, while its adoption in steering systems is devoted to guarantee high delivery pressure values. Moreover, automatic and semi-automatic transmissions may require both behaviors alternatively, in reference to the instantaneous working condition.

This brief survey on the possible behaviors required by different auxiliary systems makes evident that various design strategies must be adopted in reference to the pump specific application itself, regardless from the fact the application concerns the automotive field. Gear pumps specifically designed for the automotive industry cannot be distinguished from gear pumps for common fluid power applications on the basis of simple considerations on the ratio between the delivery pressure and the outlet flow rate. The peculiarity of such a machine category is given by the compelling need to accomplish the necessary working characteristics together with other essential constraints related to weight and global size minimization, mechanical efficiency maximization and Noise, Vibration and Harshness (NVH) behavior improvement.

In order to achieve these goals, many distinctive solutions are nowadays considered and evaluated along the design process. In conventional applications, the pump is driven by an electric motor which makes it operating at constant nominal conditions defined by speed and delivery pressure. However, contemporary needs to reduce weight and size of auxiliary systems forces gear pumps to be driven by the engine instead and to work smoothly within a wider range of speed. Moreover, it is becoming more desirable to run pumps at higher speeds to deliver lubricant at much higher flow rates rather than increasing their displacement.

Since the volumetric machine delivery flow rate directly depends on the pump theoretical displacement and the working speed, the design process can follow two different philosophies to increase it. The first option is to increase the pump displacement; this solution can be easily achieved, for example, by increasing the gear facewidth. However, this choice leads to a considerable increment of both size and weight. On the other hand, the second option concerns the increase of the pump working speed. Such a design layout, which allows for a considerable reduction of the global dimension of the auxiliary system and the pump itself, is easily obtained by connecting the pump to the Internal Combustion (IC) engine by means of a multiplier gearbox. The gearbox does not substantially alter the behavior of the pump, while it makes possible for the volumetric machine to reach higher speed values, usually above the $6000\mathrm{rpm}$, even if the IC engine does not overcome the $4500\mathrm{rpm}$ limit.

As one can well imagine, the adoption of the IC engine to drive the pump comes also together with some negative aspects. The volumetric machine is forced to work throughout a considerably wide speed range and, therefore, it must be designed to properly perform at several different working conditions. Moreover, such a characteristic becomes more and more challenging as the speed range increases: many major design parameters, e.g. relief/lateral groove shape and width, radial/axial clearances, may have different optimum solutions between the low speed condition and the high speed one. The relief groove size, in particular, has a deep influence on the fluid-dynamic behavior of the pump and its optimal design may strongly depend on the working speed condition. At low nominal speed, the relief groove size can be kept as close as possible to the best theoretical one [7] to ensure high levels of delivery flow rate regularity without undesired overpressure phenomena. On the contrary, as the speed is increased, its width should be reduced in order to avoid high pressure peak phenomena inside the trapped volume [8]. In this context, a high efficiency and reliable pump can be obtained by modifying both teeth and relief groove shape [9], so that the pump guarantees high volumetric efficiency at low speed and reduced overpressure peaks as it starts running faster. However, such a result cannot be achieved by following basic design rules; on the contrary, it is the successful outcome of a design process based on trial and error, analytical and empirical design correlations, as well as many numerical and experimental evaluations.

In a similar manner, the choice to reduce pump weight and global size by raising the working speed may give birth to undesired phenomena and it has to be pursued with a proper plan. The speed increasing, as in many other fluid power machines, may promote cavitation incipience and considerably worsen the NVH behavior of the entire pump. The first scenario is usually due to the oil flows discharged from the trapped volume to the inlet chamber: by increasing the working speed, the mean velocity of such flows is increased both because of the gear pair angular speed increment and because of the high pressure peak increasing. The consequence is a sudden drop of the pressure value at the inlet side of the meshing zone, which causes the appearance of air release and vaporization phenomena. The following collapse of the bubbles dragged from the inlet chamber to the outlet one produces intensive wear and corrosion, even if cavitation is just at incipient stage. Once cavitation is fully developed, a second effect is recognized: gear pockets moving from the suction chamber to the delivery one start being chocked by gas and vapor, producing a sharp drop of the volumetric efficiency. Finally, cavitation is also responsible for a consistent increment of the oil pressure ripple amplitude and a consequent deterioration of the pump NVH characteristics.

Risks related to cavitation are taken to extremes by considering that its practical characterization, independently whether it is faced experimentally or numerically, is typically a challenging task. Regarding the experimental approach, the early detection of cavitation cannot be performed with standard measurements based on efficiency evaluation. The delivery flow rate, as already demonstrated in refs. [10, 11], represents a good indicator of the fully developed condition; however, it is not capable to accurately describe the evolution of the phenomenon from the incipient stages. A monitoring system to properly detect incipient cavitation, which can be as harmful as fully developed cavitation, usually requires the adoption of acoustic emission sensors, hydrophones or particle-image velocimetry approaches, together with dedicated post-processing techniques. In gear pumps for automotive purposes, the detection becomes even more challenging since the machine is generally installed inside a tank, working in submerged condition. On the other hand, numerical models including cavitation are still not so widespread in industrial research, probably due to their characteristics of requiring a full definition of the oil physical properties with respect to both temperature and pressure values, as well as to their negative features of being unstable and time consuming.

As it will be enlightened in Chapter 2, the speed increasing may negatively affect the pump NVH behavior even if cavitation does not actually occur. Shifting the working range towards higher speed values means moving the main excitation frequency, which corresponds to the gearpair mesh frequency, towards higher values. As the main excitation frequency increases, the frequency content of its harmonics raises proportionally. Therefore, the velocity incrementation expands the frequency range influenced by the main excitation harmonics, with the potential effect of including a major number of resonances. Since gear pumps are usually characterized by resonances with high frequency values and a limited number of teeth, as analyzed in Chapter 2, if the working speed is kept as low as possible, such resonances are excited by high order harmonics with a limited amplitude. If the speed is sufficiently increased, low order harmonics start crossing the main natural frequencies producing negative effects not only on the emitted noise, but also on the mesh force and the loads applied to the bearings.

The influence of these phenomena may be reduced by taking advantage of the benefits provided by helical gears. As it is well known, helical gears are characterized by a higher contact ratio and a smoother working behavior, making them a desirable design solution for high speed gear pumps [12]. On the other hand, as already underlined in ref. [13], helical gear pumps feature lower displacement values and higher outlet flow ripple irregularity if compared to spur gear pumps of the same size. Moreover, both positive and negative effects get stronger as the helix angle is increased. From a practical point of view, helical gears may produce a global positive outcome in applications concerning low to medium loads and high speed values; however, it is clear that their adoption requires a careful evaluation of various contrasting effects.

Despite gear pumps can be considered as basic devices, this brief survey enlightens how the design becomes rather complex for them to achieve the primary goal of delivering high-pressure flow while meeting requirements for higher efficiency, lower noise levels and reduced size. Many design solutions, involving both technological and physical aspects, may be adopted; nevertheless, no straight path is available to obtain the desired performances and the design process may result to be considerably expensive. Within this framework, it is clear the need to define a set of reliable tools to assist designers at each step of the design course, i.e. tools providing accurate predictions with respect to the set of geometrical parameters actually known at the reference design step. In order to clarify this idea, one may refers to the different needs characterizing subsequent phases of the design process. Early stages do not take advantage of high accuracy models requiring large sets of geometrical and physical parameters to analyze a single working condition. Within these steps, the level of uncertainty related to several parameters makes the results provided by such models to be meaningless and, above all, useless. On the contrary, the possibility to predict global trends and macro numbers would be much more profitable since they can give fundamental knowledge regarding which design choice should be examined in depth. As a direct consequence, reduced models with a limited number of Degrees of Freedom (DOFs), but still capable to point out the design parameters governing the phenomenon, have to be preferred. These models become even more appealing by considering that wide ranges of working conditions and parameters values can be analyzed with a limited computational effort. By following the same philosophy, later design steps are usually focused on optimizing the machine behavior by slightly refining some crucial parameters. Within this context, highly accurate predictions become mandatory and they have to be performed with numerical models specifically built up to study peculiar phenomena, e.g. interaction between gear radial positioning and bearing reactions. The need of different approaches could be summarized by considering that during the first design stages, parameters need to be investigated in terms of their order of magnitude, while advanced stages are devoted to the precise tuning of the machine, which is pursued by looking for the optimum value of each parameter inside a small neighborhood.

1.2 OVERVIEW OF THE THESIS

On the basis of the various needs pointed out in the previous section, the present manuscript describes three different methods for studying the performance of gear pumps, by taking into account critical aspects as weight and size reduction, NVH improvements, helix influence, non-unitary transmission ratio gearpairs and presence of cavitation, which are solutions currently faced by automotive applications. In particular, two models are dedicated to the analysis of the pump behavior with respect to a specific field of interest, ranging from the dynamics of the gearpair to the efficiency of the volumetric machine itself. Since the reliability of the simulated results represents a central feature for every numerical model, dedicated experimental campaigns are associated to each modeling approach. The third approach is focused on addressing cavitation promoted by high speed conditions and it is purely based on experimental tests and post-processing of the measured data. The following is a brief overview of the chapters.

Chapter 2 is devoted to the description of a nonlinear dynamic model adopting a Lumped Parameter (LP) approach. The aim of the model is to provide a simulation tool based on a limited number of design specifications, in order to capture the essential characteristics defining the pump dynamics. Such a modeling approach represents a novel method with respect to the one already introduced in literature, whose purpose is the high accuracy estimation of the pump NVH behavior based on the full definition of the machine geometry. In particular, the present model allows to focus the attention on the set of design parameters that mainly influence the phenomenon, avoiding so the need to take into account a number of design specifications that have a secondary relevance in its definition. For this reason, variable pressure loads are calculated by using an analytical approach based on simplifying but realistic hypotheses; on the other hand, speed dependent drag torque is obtained by applying regression techniques on measured data. As a direct consequence of the considerations reported in section 1.1, the model is a valuable tool to predict the dynamics of the pump at early steps of the design process.

Results obtained from a parametric study are also presented and discussed, pointing out the effects of various design choices, e.g. relief groove dimension, lateral grooves extension, with respect to a wide range of operating conditions. In particular, such results have shown that the pressure value reached inside the trapping zone has a deep influence on the dynamic behavior of the pump, in particular in the high speed range, where the fifth natural mode can be excited by low order harmonics of the mesh frequency. The analysis suggests that careful attention should be paid in the design process of a gear pump working through a wide speed range, since the relief groove must satisfy contrasting requirements. Low speed conditions require an increase of the relief groove width to guarantee high efficiency values, while high speed conditions require to reduce it in order to avoid high pressure phenomena in the trapped volume. The pressurizing zone extension has been also taken into account during the analysis, showing that different widths of the pressurizing zone lead to different orientations of the pressure force without affecting its amplitude. For this reason, this design characteristic may have a major influence on the static component of the bearing reaction and meshing force, while the dynamic behavior of the pump is not altered.

In Chapter 3, a LP model developed to predict gear pump performances in terms of volumetric efficiency and pressure dependent phenomena is introduced. In contrast with the minimal model described in Chapter 2, the present approach is focused on evaluating the effects of slight design modifications, by taking into account a wide range of design specifications. In order to achieve this goal, the model is able to include the presence of helical gears, as well as gearpairs with non-unitary transmission ratio and arbitrary shaped relief/lateral grooves. Discharge coefficients, that are usually taken from ref. [14] and then slightly adjusted to reach a better experimental validation (see for example ref. [15]), have been determined with the help of Computational Fluid Dynamic (CFD) codes. The main innovative characteristic of the proposed LP model is the coupling with a novel set of simplified equations of motion of the gearpair, allowing for the calculation of the gears micromotions as a result of the instantaneous balancing between the simultaneous presence of variable pressure loads, a speed dependent drag torque, the meshing force and the bearing reaction. Although this modeling approach requires a considerable amount of data referring to the pump geometry and the oil physical properties, it allows for the prediction of the instantaneous radial clearances and, consequently, for an accurate estimation of the volumetric efficiency of the pump.

A large part of Chapter 3 is devoted to the description of a systematic procedure developed to determine variable excitation loads coming from pressure evolution inside tooth pockets. The purpose of the procedure is to clearly define an accurate and flexible methodology that can be easily implemented in different calculus environments and straightforwardly applied to both simulated and measured pressure data, in a wide variety of gear pumps. The originality of the outlined method lies in the capability to analyze both spur and helical gearpairs, by determining all the spatial components of the pressure loads. By comparing loads estimated by the proposed methodology with loads calculated by two other methods described in refs. [16, 17], the proposed procedure results capable to take into account a wider range of phenomena occurring inside the meshing zone, thanks to a more accurate discretization of the meshing course. A considerable increase of accuracy is reached also in the determination of the pressure torque applied to each gear center, since it mostly depends on the oil pressure inside the trapped volume.

Reliability and accuracy of the estimation, as well as the model sensitivity to parameters modification, is assessed by comparing simulated results with an extended set of measured data. The experimental campaign, in particular, is performed on a set of 20 nominally identical pumps. Actual clearances at the end of the production process have been measured for each sample; later, such pumps have been tested on a wide range of operating conditions, in order to check the model response with respect to various working speeds, delivery pressure values and oil temperatures. The comparison shows that the proposed model can guarantee high accuracy predictions in terms of pump volumetric efficiency throughout the entire range of working conditions considered. Concurrently, model sensitivity to slight design modifications is comparable to the real pump behavior.

Chapter 4 deals with the development of an experimental procedure to early-detect cavitation in gear pumps working at high speed values. The phenomenon has been rarely studied and no experimental data can be found in the specialized literature, where just few numerical studies have been published. For this reason, cavitation in gear pumps is firstly experimentally characterized, with the help of both efficiency and vibro-acoustic measurements. Then, an *ad hoc* methodology is settled up in order to evaluate cavitation throughout its entire evolution, from the incipient condition to the fully developed one. Results obtained from the signal processing of different sensors such as accelerometers, hydrophone and pressure pulsation transducers are shown and discussed. Effect of oil temperature is also investigated, showing that it contributes in spreading the phenomenon on a wider speed range.

Finally, last Chapter is devoted to concluding remarks.

2

A NONLINEAR DISCRETE DYNAMIC MODEL OF GEAR PUMPS

The chapter presents a mathematical model describing dynamic behavior of gear pumps throughout a wide speed range is presented in this paper. This transverse-torsional model accounts for the bearing compliance and gear backlash non-linearity. Dynamic loads due to the pressure distribution around the gears are estimated by means of an analytical procedure, as well as speed-dependent drag torque caused by leakages. Modal characteristics of the dynamic system are discussed, showing that common design features of typical gear pumps such as a low number of teeth, a facewidth-to-tip diameter aspect ratio close to one, and restricted speed range do not allow for the first harmonic of mesh frequency excitation to excite the main natural modes. The proposed model is used to perform parametric studies on the effects of different outlet pressures, presence of speed-dependent high-pressure peaks in the trapping volume, and various pressurizing zone extensions. Results indicate that the pressure value reached inside the trapping zone has a significant influence on the dynamic behavior of the pump, particularly in the high-speed ranges, where the fifth natural mode can be excited by higher harmonics of the mesh frequency.

2.1 INTRODUCTION

The majority of the numerical studies referring to gear pumps concentrated on evaluating the influence of various design aspects on volumetric and mechanical efficiencies of the pump, while ignoring their dynamic consequences, which dictate the noise performance of the pump. There is a limited number of published works focusing on dynamics of a gear pump. For instance, Mucchi et al. [17, 18] proposed a complete procedure for performance improvement of pump prototypes starting from the calculation of the pressure course around the gears. Later, the same procedure was validated through experimental comparisons and was extended to helical gears [19], showing the benefits obtained by increasing accuracy of the estimation of the pressure ripple inside the gears [16]. Effects of some of the key design parameters, namely radial clearance and relief groove dimension, and different working conditions including oil dynamic viscosity and delivery pressure, were evaluated [20]. However, these analyses have been limited to low-speed conditions, from $1500\mathrm{rpm}$ to $3500\mathrm{rpm}$, ensuring the absence of high-pressure phenomena inside the trapped volumes. Other studies pertaining to the same authors have been presented on this subject: in particular Dalpiaz et al. [21] proposed a procedure for the experimental verification of the model introduced in [17, 18], while Mucchi et al. [22] employed Finite Element (FE) and Boundary Element (BE) analyses to define a procedure for evaluating the vibration of the pump casing as well as the emitted noise.

Dynamics of a gear pump can be treated the same way as gear pair dynamics. Nonlinear gear pair models with backlash have been proposed since the early $90'$s [23, 24, 25, 26, 27] some of which were correlated to measurements [28, 29]. The coupling between transverse and torsional motions at the gear mesh were also included in cases when gear supports are flexible [24], in the process effects of rolling-element and journal bearings can be evaluated [26, 30]. Finite element models of gear shafts were incorporated in refs. [31, 32] to couple motions of the shafts via a gear mesh. Several other studies looked into analyzing dynamics of geared systems under various conditions, including shape deviations, mounting errors or engine speed fluctuations [33, 34].

In applying these well-established gear dynamics models to gear pumps, one must take into account several unique aspects of a gear pump. In particular, the presence of pressure-dependent external forces, speed-dependent friction torque and the absence of external loads connected by the output shaft to the driven gear all play an important role in determining the overall pump dynamics. Within this context, this present work focuses on studying the dynamics of gear pumps in a wide speed range, taking into account the influence of design parameters such as angular extension of the pressurizing zone, backlash value and presence of high level and speed dependent pressure peaks inside the trapping zone. Particular attention is given to the meshing force and bearing reactions, as they are considered to be the main structure-borne excitations that, together with the fluid-borne excitations given by the oil pressure ripple, load the pump housing.

The works from [17] to [22] regards modeling techniques for performance evaluation and improvement of arbitrary but specific gear pump prototypes. On the contrary, the current study is focused on defining a set of equations to describe the dynamics of gear pumps as it is influenced by some design characteristics that are common peculiarities for this family of machines. With this purpose, the present work introduces a different set of dynamic equations with respect to the one described in [17], by taking into account the modeling of a speed dependent friction torque component. Variable pressure loads are analytically estimated, by introducing a novel procedure that allows for a sufficiently accurate estimation of the pressure force applied to the gears on the basis of realistic hypotheses. In comparison to the analytical approach proposed in [3, 17], the present one has the major advancement to include the effects caused by possible pressure peak phenomena in the trapped volume. Moreover, the analytical estimation is extended to the determination of all the pressure force components, while in previous studies it was limited to the calculation of the pressure torque.

By following this approach, the current study faces off the modeling of the gear pump dynamics on a different perspective from the one proposed in previous works. In particular, a minimal model has been developed to estimate the dynamic behavior of gear pumps at the early stage of the design process, when the pump geometry is not completely defined. As a matter of fact, in this design stage various design parameters, e.g. pump radial clearances, bearings radial clearances, lateral clearances, relief groove shape and dimension, are not already determined and, consequently, there is no chance to simulate the pump behavior by using advanced approaches as the ones described in [35, 3, 17, 2]. Hence, the proposed model is intended to serve as a computationally efficient design assessment tool that is sufficiently accurate with respect to the limited number of design parameters required to run the simulations. The accuracy of the present approach will be discussed in the Chapter, by comparing the pressure loads calculated with the present procedure with the results obtained with more advanced methods.

The following Section proposes the mathematical model, while Section 2.3 concentrates on the estimation of variable-pressure loads based on a simplified analytical approach that is capable of taking into account high-pressure phenomena occurring inside the trapped volume as well as defining the modeling of the friction torque behavior. Section 2.4 presents results of the proposed non-linear dynamic model, focusing on modal characteristics of the linearized unloaded model and the forced response in the form of gear mesh force and bearing reactions caused by high levels of pressure inside the trapped volume. Finally, the last section is devoted to concluding remarks.

2.2 DYNAMIC MODEL

A discrete dynamic model of a gear pump is presented in Figure 1. It consists of two gears of typically the same number of teeth, each represented by rigid disks and supports and their respective shafts, each one supported by a pair of journal bearings. An Internal Combustion Engine (ICE) usually drives the pump by means of a flexible joint. Since the inertia of the pump is considerably smaller than that of the ICE, the engine can be replaced with a fixed frame connected to the driving gear by a flexible shaft. This modeling solution is also allowed by the fact that the frequency range typically influenced by the first harmonics of the crankshaft angular speed is considerably lower than the frequency range that characterizes the first harmonics of the gear pump mesh frequency. Each gear *i* (*i=1,2*) is allowed to vibrate along the transverse plane of the gears and vibrate torsionally about its nominal rigid rotation $\vartheta_i = \omega_i t$ where ω_i is the nominal rotational speed of gear *i*. The 6-degree-of-freedom non-linear dynamic model of Figure 1 leads to the following equation of motion:

$$\left.\begin{aligned}
&m_1\ddot{x}_1 + k_{xx1}x_1 + k_{xy1}y_1 + F_{px}^{(1)} = 0\\
&m_1\ddot{y}_1 + k_{yx1}x_1 + k_{yy1}y_1 + F_{py}^{(1)} + F_m = 0\\
&J_1\ddot{\theta}_1 + k_s\theta_1 - r_1F_m + T_d^{(1)} - T_p^{(1)} = 0\\
&m_2\ddot{x}_2 + k_{xx2}x_2 + k_{xy2}y_2 + F_{px}^{(2)} = 0\\
&m_2\ddot{y}_2 + k_{yx2}x_2 + k_{yy2}y_2 + F_{py}^{(2)} - F_m = 0\\
&J_2\ddot{\theta}_2 - r_2F_m + T_d^{(2)} - T_p^{(1)} = 0
\end{aligned}\right\} \tag{1}$$

where the damping terms have been neglected for sake of clarity. x_1 and x_2 are the translational motions of gears normal to the gear mesh line of action, y_1 and y_2 are translational motions along the line of action, and θ_1 and θ_2

are the rotational vibrations about the nominal rotational angles ϑ_1 and ϑ_2, respectively. Terms m_i, J_i and r_i denote mass, polar mass moment of inertia and the base radius of gear *i*, respectively. k_{xxi}, k_{xyi}, k_{yxi} and k_{yyi} are the stiffness components of the journal bearing supporting gear *i*. As proposed in ref. [24], the gear mesh force $F_m(t)$ is defined by taking into account the backlash clearance of $2\bar{x}_b$ as

$$F_m(t) = \begin{cases} k_m\left[x_r(t) - \bar{x}_b\right] & x_r(t) \geqslant \bar{x}_b \\ 0 & |x_r(t)| < \bar{x}_b \\ k_m\left[x_r(t) + \bar{x}_b\right] & x_r(t) \leqslant -\bar{x}_b \end{cases} \tag{2}$$

where k_m is the average value of the gear mesh stiffness. The time variance of mesh stiffness is considered secondary due to the light loads in relation to the gear pair size and the fact that the gear pair is always very close to unity ratio. $x_r(t)$ is the relative gear mesh displacement defined as

$$x_r(t) = [y_1(t) - r_1\theta_1(t)] - [y_2(t) + r_2\theta_2(t)] \tag{3}$$

In Eqn. 1, $F_{px}^{(i)}$ and $F_{py}^{(i)}$ are the components of the pressure force vector $\mathbf{F}_p$ caused by the pressure distribution around gear *i*, $T_p^{(i)}$ is the variable torque caused by the unbalanced pressure inside the trapping zone, and $T_d^{(i)}$ is the friction torque acting on gear *i*. Dynamic systema in Eqn. 1, together with the damping terms, can be written in matrix form to obtain

$$\mathbf{M}\,\ddot{q} + \mathbf{C}\,\dot{q} + \mathbf{K}\,q + \mathbf{T}_d = \mathbf{F}_p \tag{4}$$

where $\mathbf{M} = Diag\begin{bmatrix} m_1 & m_1 & J_1 & m_2 & m_2 & J_2 \end{bmatrix}$

$$\mathbf{q} = \begin{bmatrix} x_1 \\ y_1 \\ \vartheta_1 \\ x_2 \\ y_2 \\ \vartheta_2 \end{bmatrix} \tag{5}$$

$$\mathbf{K}=\begin{bmatrix} k_{xx1} & k_{xy1} & 0 & 0 & 0 & 0 \\ k_{yx1} & k_{yy1}+k_m & -r_1k_m & 0 & -k_m & -r_2k_m \\ 0 & -r_1k_m & r_1^2k_m+k_s & 0 & r_1k_m & r_1r_2k_m \\ 0 & 0 & 0 & k_{xx2} & k_{xy2} & 0 \\ 0 & -k_m & r_1k_m & k_{yx2} & k_{yy2}+k_m & r_2k_m \\ 0 & -r_2k_m & r_1r_2k_m & 0 & r_2k_m & r_2^2k_m \end{bmatrix} \tag{6}$$

$$\mathbf{T}_d=\begin{bmatrix} 0 \\ 0 \\ T_d^{(1)} \\ 0 \\ 0 \\ T_d^{(2)} \end{bmatrix} \tag{7}$$

$$\mathbf{F}_p(t)=\begin{bmatrix} F_{px}^{(1)} \\ F_{py}^{(1)} \\ T_p^{(1)} \\ F_{px}^{(2)} \\ F_{py}^{(2)} \\ T_p^{(2)} \end{bmatrix} \tag{8}$$

The definition of the damping matrix **C** in Eqn. 4 is discussed in Section 2.4.2. Time-varying forcing vectors $\mathbf{F}_p$ and $\mathbf{T}_d$ form the excitations for the system and they will be defined in the next section.

It is worth noting that the off-diagonal bearing stiffness terms k_{xyi} and k_{yxi} in Eqn. 6 provide coupling between the line-of-action (LOA) and off-line-of-action (OLOA) motions the same way as in refs. [24, 33] where a pair of spur gears supported by journal bearings was studied dynamically. Neglecting cross terms would eliminate any coupling between the OLOA motions, namely x_1 and x_2, and the other four degrees of freedom. The former approach may lead to more reliable results if the variable pressure loads are

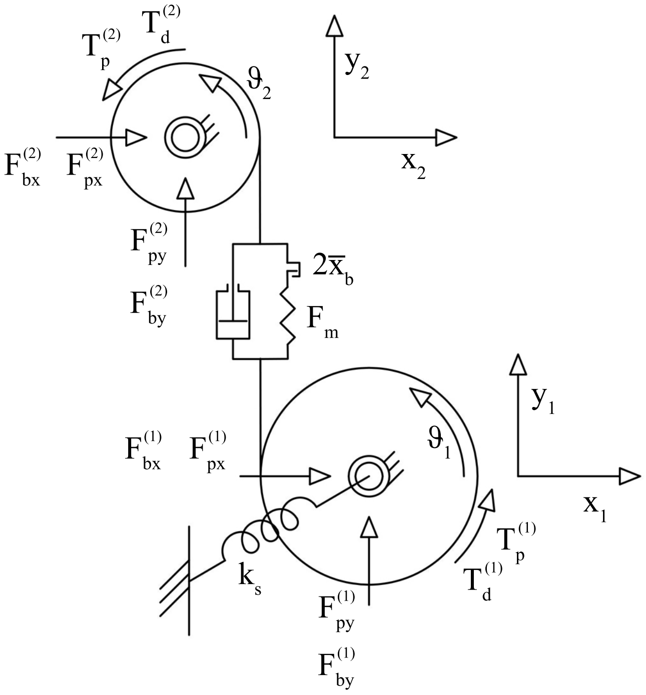

Figure 1: Dynamic model (damping associated with the shaft not shown).

estimated from fluid dynamic models used to predict the pressure distribution around the gears. As discussed in refs. [17, 35], the pressure distribution loading the two gears may vary significantly depending on the distribution of the tip clearances inside the pressurizing zone. The instantaneous positions of the two gears, therefore, influence external excitations creating a link between bearings reactions and variable pressure loads.

2.3 DEFINITION OF EXCITATIONS

The array in Eqn. 8 represents the external forces and moments induced the pressurized fluid on gears. As stated in ref. [3], the pressure distribution produces, on each gear, loads that are periodic at the gear mesh frequency. Their estimation may be obtained from direct measurements [36], lumped parameter models [17, 35] or an approximate analytical procedure. However, at the early stage of the design process, approximate analytical methods represent the only available choice; for this reason, a dedicated analytical procedure will be adopted in this study. Since results from the present study will underline the influences of the first harmonics of the mesh frequency on the dynamics of the pump, this choice does not represent a restrictive hypothesis. As already discussed in [3], the adoption of simplified analytical approaches leads to sufficiently accurate results in terms of defining general trends and describing the global behavior of pumps with common characteristics. This analytical approach assumes that the oil pressure ripple can be neglected, which is in general acceptable if sufficiently small ripple occurs with respect to the pressure drop provided by the pump. The assumption will be further addressed in Section 2.4.2. The other main assumption is that pressure inside the pressurizing zone follows a linear variation with respect to the angle. This does not affect accuracy in particular if grooves are designed to reduce the angular extension of the pressurizing zone, which is a typical feature of today's gear pumps for automotive applications. Moreover, since the result evaluation will be limited to the influence of the excitation lower harmonics, possible presence of cavitation produced by the high speed condition has been neglected. The assumption is addressed by considering that speed induced cavitation is recognized as a high-frequency broadband noise (usually above 40kHz) in the suction/delivery pressure ripple spectra. Finally, the pump is assumed to work within the typical speed range pertaining to IC engines for automotive applications. Figure 2 shows a general scheme of a gear pump for automotive applications, with the underlining shape and angular extension of both the grooves and the pressurizing zone.

The reference scheme for estimation of pressure loads applied to the driving gear (gear 1) is shown in Figure 3(a). The pressure force vectors generated inside the pressurizing zone, $\mathbf{F}^{(1)}_{seal}$, and inside the outlet zone, $\mathbf{F}^{(1)}_{out}$, are calculated by integrating the pressure in each respective zone. Their magnitudes are given respectively as

$$\left|F^{(1)}_{seal}\right| = \frac{2P_{out}r_{ext1}b}{\Delta\vartheta_{seal}}\left[\Delta\vartheta_{seal}\sin(\Delta\vartheta_{seal}) + \cos(\Delta\vartheta_{seal})\right] \tag{9}$$

$$\left|F^{(1)}_{out}\right| = 2P_{out}r_{ext1}b\sin\left(\frac{\Delta\vartheta_{out}}{2}\right) \tag{10}$$

where P_{out} is the mean delivery pressure, r_{o1} and b are the tip radius and the facewidth of the gear, respectively. $\Delta\vartheta_{seal}$ represents the angular extension

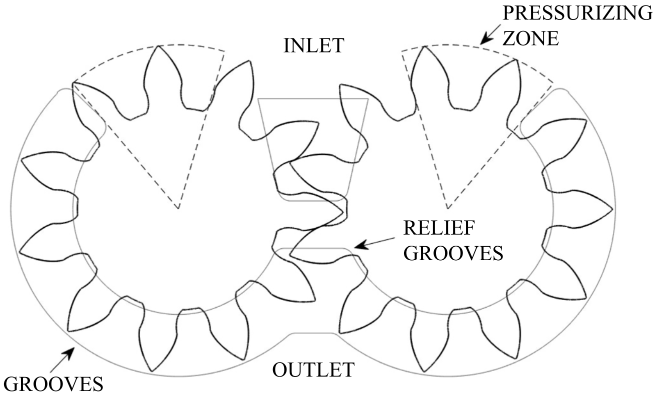

Figure 2: Typical gear pump adopted in automotive applications.

of the pressurizing zone, while $\Delta\vartheta_{out}$ describes the angular extension of the outlet zone.

The earlier assumption that the oil pressure ripple is negligible makes contributions of these two sectors time-independent. Time dependence of pressure loads originates from the contribution of the meshing zone, defined by the line of contact AD shown in Figure 3(b). Here, the line of contact is divided into three segments depending on the number of tooth pairs engaged. Segments A-B and C-D refer to the presence of two pairs of teeth in contact, thus the hydraulic sealing is provided. Segment B-C, on the contrary, refers to configuration with a single tooth pair in contact. In the instant when there is a single tooth pair in contact, the trapped volume cannot exist, and therefore, the oil pressure loading the gear pockets located on the delivery side of the contact point is set as equal to the delivery pressure. Therefore, the pressure force vector $\mathbf{F}_{stp}^{(1)}$ induced by the meshing zone has the magnitude

$$\left|F_{stp}^{(1)}\right| = 2P_{out}r_{ext1}b\sin\left(\frac{\Delta\vartheta}{2}\right) \tag{11}$$

where $\Delta\vartheta$ is the angle between the radius referred to point A and the radius of the contact point. Depending on the position of the contact point during the meshing cycle, $\mathbf{F}_{stp}^{(1)}$ changes both his magnitude and direction. When the contact point approaches point C, $\mathbf{F}_{stp}^{(1)}$ reaches its maximum magnitude and a second tooth pair starts engaging at point A. Within this framework, a trapped volume forms between the two contact points, one within A-B and one within C-D, and the pressure of the oil captured inside it either rises considerably or stays equal to the outlet pressure depending on different factors, such as relief groove dimensions, backlash value, and angular speed [8]. Adopting the scheme shown in Figure 4, the magnitude of $\mathbf{F}^{(1)}_{trap}$ caused by the oil pressure inside the trapped volume P_{trap} is defined as

$$\left|F^{(1)}_{trap}\right| = 2P_{trap} r_{\vartheta 1} b \sin\left(\frac{\vartheta_1 - \vartheta_2}{2}\right) \tag{12}$$

Also noted in Figure 4 when two tooth pairs are engaged, another pressure force component loads the angle spanned by ϑ_2. Since the oil pressure within this sector is equal to P_{out}, the corresponding pressure force is calculated by using Eqn. 11, with ϑ_2 in place of $\Delta\vartheta$. Once all fluid pressure forces acting on gear 1 are defined, the total fluid force $\mathbf{F}^{(1)}_p$ is found as the sum of $\mathbf{F}^{(1)}_{seal}$, $\mathbf{F}^{(1)}_{out}$ and $\mathbf{F}^{(1)}_{stp}$ or $\mathbf{F}^{(1)}_{trap}$ (depending on number of tooth pairs in contact). In particular, since the pressure forces defined above act along the radial direction, their components along axes x and y must be determined before Eqn. 8 can be populated by $F^{(1)}_{px}$ and $F^{(1)}_{py}$. However, considering that for each pressure force both magnitude and line of application are known, this last part of the procedure does not require a considerable computational effort. The same procedure is used to determine fluid pressure forces $F^{(1)}_{px}$ and $F^{(1)}_{py}$ acting on gear 2. It is noted that the pressure force components created at the pressurizing and outlet zones are considered to be constant while the pressure force components inside the trapping zone depend on the position of the contact point. As such, they must be reevaluated at each rotational position increment [3].

The pressure distribution around the gears not only creates the forces defined above but also produces a time-varying pressure torque. While gear pockets outside the trapping zone can be considered tangentially balanced by assuming a constant pressure inside each one, an unbalanced pressure force component along the tangential direction is produced due to the meshing action, in the process, causing torque, as explained in ref. [3, 17]. An analytical derivation of this pressure torque, $T^{(1)}_p$, taking into account the presence of overpressure peaks inside the trapped volume was provided in ref. [16], showing that the contribution of the oil pressure inside the trapped volume must also be included for achieving required accuracy. As done for estimating pressure force created at the trapping zone, calculation of $T^{(1)}_p$ is done in two consecutive steps, depending on the number of tooth pairs in contact. According to Figure 3, when a single tooth pair is engaged, $T_p^{(1)}$ is defined as

$$T_p^{(1)} = \frac{1}{2} P_{out} b (r_{ext1}^2 - r_{\vartheta 1}^2) \tag{13}$$

When there are two tooth pairs in contact, the pressure torque is defined with respect to Figure 4 as

$$T_p^{(1)} = \frac{1}{2} b \, (P_{out} - P_{trap})(r_{ext1}^2 - r_{\vartheta 1}^2) + \frac{1}{2} b \, P_{trap}(r_{ext2}^2 - r_{\vartheta 2}^2) \tag{14}$$

As the pressure forces produced inside the trapping zone, $T_p^{(1)}$ is also time dependent, as well as $T_p^{(2)}$ that is defined the same way, requiring evaluation at each rotational position increment.

Meanwhile, $\mathbf{T}_d$ in Eqn. 4 represents the resisting torque produced within the pump. As already described in [37, 38] by means of experimental evidence and mathematical models, torque loss in volumetric machines mainly depends on oil physical properties, working speed and delivery pressure. In particular, as shown in [39], torque $\mathbf{T}_d$ can be divided in three main contributions:

$$T_d = T_{d\mu}(\mu, \omega) + T_{d\rho}(\mu, \omega^2) + T_{dp}(\Delta p) \tag{15}$$

where $T_{d\mu}$ accounts for losses due to laminar flows, showing a linear dependence from the working speed and the oil dynamic viscosity, and $T_{d\rho}$ accounts for losses due to turbulent flows, with a quadratic dependence from the speed and linear dependence from the oil density, e.g. journal bearings, tooth tips and casing. Finally, $T_{d\rho}$ mainly depends on the delivery pressure since it accounts for losses originated from parts of the pump where there are instances of dry friction. However, as shown in [37], pressure difference may have a limited influence on the overall resisting torque T_d if its variation is limited to $30 - 40 bar$.

On the basis of the above considerations, torque $T_d^{(i)}$ acting on gear *i* is expressed in terms of its angular speed ω_i as

$$T_d^{(i)} = c r_i^2 \omega_i \tag{16}$$

Here coefficient *c* substantially takes into account all the contributions defined in Eqn. 15 and its value can be estimated by using numerical approaches (as

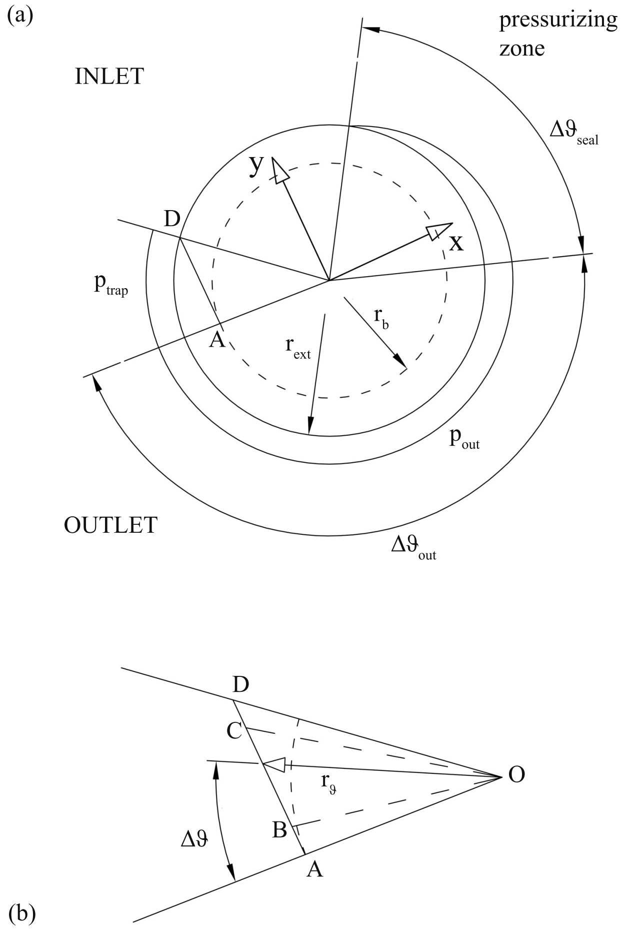

Figure 3: Reference scheme to calculate the pressure loads applied to the gears (a) and (b) effects produced in the trapped zone, where segment DA is the line of contact.

the one proposed in [39]) or by using experimental measurements. In the latter case, by assuming that in steady state conditions, for each working point, the following equation can be applied

$$T_e\bar{\omega} = \frac{1}{\eta_v}\Delta P Q_{out} + 2T_d\bar{\omega} \tag{17}$$

Hence, by measuring the driving torque T_e, the mean angular speed $\bar{\omega}$, the pressure difference between inlet and outlet chamber ΔP and the outlet flowrate

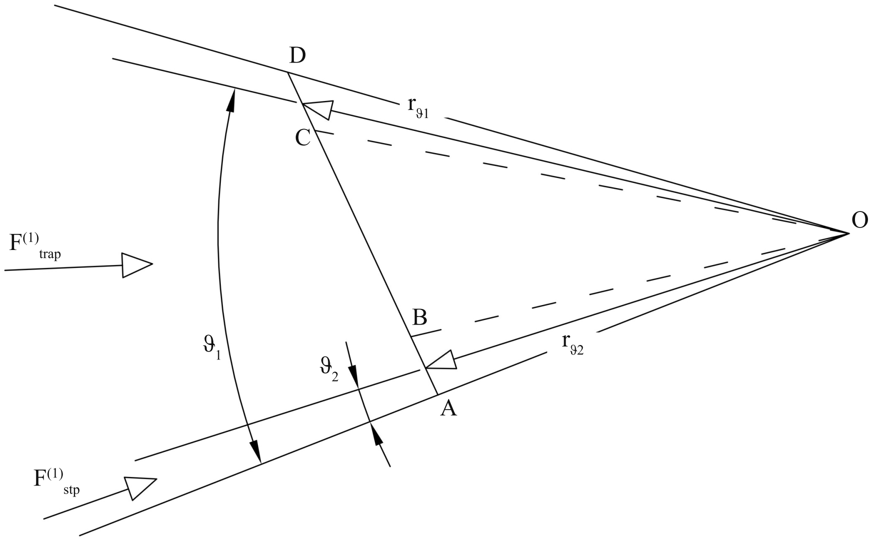

Figure 4: Pressure force, when two tooth pairs are simulateneously engaged. Points A and D define the length of the contact line.

Q_{out}, which are quantities commonly measured in gear pump performance tests, it is possible to determine the drag torque T_d and therefore, by Eqn. 16, the value of coefficient *c*. Such tests must be repeated for a number of different working speed in order to estimate *c* in reference to the actual working condition. On the basis of the theoretical assumptions leading to Eqn.15, for a given delivery pressure, coefficient *c* can be written mathematically as

$$c = a_1 \omega_i^{-a_2} + a_3 \tag{18}$$

where a_1, a_2 and a_3 are positive coefficients that are defined experimentally by using common regression techniques, e.g. least squares method, applied to set of measured data taken at different working speed conditions.

2.4 RESULTS AND DISCUSSION

In the present section, results obtained by the dynamic model described in Section 2.2 will be shown and discussed, focusing attention on meshing force and bearing reaction caused by variable pressure loads, within a wide speed range. With this purpose, subsection 2.4.1 addresses the modal characteristics of the linearized dynamic model while subsection 2.4.2 points out the influence of design parameters on meshing force and bearing reaction force. Within this context, effects produced by angular extension of the pressurizing zone and presence of speed dependent pressure inside the trapped zone will be discussed.

The dynamic model presented in Section 2.2 has been implemented in Matlab environment. As underlined in [40], non-linear dynamic models of a gearpair need to be solved with extremely small integration steps, of the order from 10^{-4} to 10^{-7}, since rattle impacts between gears may take place within a very small interval. Moreover, double precision calculation is compulsory in order to ensure accurate simulations. However, nowadays these are not tricky requirements anymore, since the computational performance of modern laptop computers is sufficient to deal with these problems without a considerable effort.

In order to carry out this study, a gear pair constituting the pump core has been designed coupling basic design rules with Eqn. 19, which is used to correlate a gear pump design characteristics with the pump displacement $\bar{Q}_d$ [41]:

$$\begin{aligned}\bar{Q}_d \quad = \quad & \frac{z_1 b}{2}\left[r_{ext1}^2 + \tau r_{ext2}^2 - r_{o1}\left(r_{o1} + r_{o2}\right)\right] + \\ & -\frac{z_1 b}{2}\left[(1+\tau)\left(\frac{r_{\vartheta start}^2 + (p_b - p_b \varepsilon)^2 + (p_b - p_b \varepsilon)\, r_{\vartheta start}}{3}\right)\right] \qquad (19)\end{aligned}$$

where τ is the transmission ratio, p_b represents the gearpair base pitch and ε is the contact ratio; term $r_{\vartheta start}$ describes the radius of the driving gear at the start of active profile, i.e. the tooth profile actually in mesh. The gear pair of the example pump has no profile shift and $\tau = 1$; Eqn. 19 is used to determine the face width b for a given $\bar{Q}_d$.

The designed gear pump has been taken as reference for the analysis that will be shown in subsection 2.4.1 and 2.4.2. Table 1 shows the main design characteristics of the adopted gear pair; all the other gearpair parameters can be deduced from Table 1 by following standard gear design rules.

Table 1: Gear pump main design parameters

Pump Displacement	$6 cm^3/rev$
Tooth number $z_{1,2}$	14
Normal module m_n	$2.8 mm$
Pressure angle α	25°C
Base radius r	$17.5 mm$
Facewidth b	$40 mm$
Driving gear mass m_1	$0.564 kg$
Driven gear mass m_2	$0.414 kg$
Driving gear inertia J_1	$8.14 * 10^{-5}\ kgm^2$
Driven gear inertia J_2	$7.22 * 10^{-5}\ kgm^2$
Mesh stiffness k_m	$6.14 * 10^8\ N/m$
Shaft length	$50 mm$

2.4.1 *Modal characteristics*

The definition of the modal characteristics of the dynamic system is a first step towards characterizing the forced response of the system. In order to carry out this analysis, bearing stiffness matrix has been defined on the basis of the experimental and numerical data reported in Refs. [42, 43] for full circular bearings. It is worth noticing that bearing stiffness terms $k_{xx}, k_{yy}, k_{xy}, k_{yx}$ depend on the actual relative eccentricity e and their value may vary consistently as e moves from zero to one. However, by considering that in gear pumps the relative eccentricity values usually lay in a restricted range between 0.85 and 0.95, as underlined in Refs. [17, 20], bearing stiffness terms can be considered as constants and defined by Eqns. 20 and 21:

$$\mathbf{K}_b^1 = \begin{bmatrix} k_{xx} & 0.5k_{xx} \\ 0.1k_{xx} & 0.1k_{xx} \end{bmatrix} \tag{20}$$

$$\mathbf{K}_b^2 = \begin{bmatrix} k_{xx} & -0.5k_{xx} \\ -0.1k_{xx} & 0.1k_{xx} \end{bmatrix} \tag{21}$$

It is worth noting that Eqns. 20 and 21 refer to the case in which the direction of the applied load coincides with axis x; if this assumption is not verified, matrices $\mathbf{K}_b^1$ and $\mathbf{K}_b^2$ must be rotated accordingly. By assuming $k_{xx}/k_m = 0.1$, six coupled transverse-torsional normal modes are predicted as shown in Figure 5. Figure 5(a) shows the first mode, in which the driven gear vertically translates and rotates in opposite direction while the driving one is almost unperturbed, leading to a negligible variation of the relative displacement x_r. Concurrently, the driven gear shows a consistent translation along the horizontal direction, demonstrating that the first mode is mostly related to the journal bearing supporting the gear. The second mode, shown in Figure 5(b), is mainly characterized the translation in both vertical and horizontal direction of the driving gear, while the in-phase rotation of the driven one leads to a negligible variation of the relative displacement x_r. In analogy to the first mode, the second one is mainly due to the journal bearing supporting the driving gear. Figure 5(c) shows the third mode, in which the two gears translate vertically and rotate in opposite directions, leading to a small but still appreciable variation of the relative displacement x_r, horizontal translation is negligible for both the gears. The fourth mode, shown in Figure 5(d), is defined by in-phase vertical translations of the two gears, while a slight rotation in the opposite direction eventually leads to a small relative gear mesh displacement; a small horizontal translation of the driven gear is appreciable. The fifth natural mode in Figure 5(e) similar to the third, is given by a combination of vertical translations and rotations that are in opposite directions. It is worth noting that this natural mode can be observed only because the model takes into account the shaft connecting the engine to the gear pair, leading to a definite system. For the same reason, the natural frequency associated to the fifth mode strongly depends on the torsional stiffness of the input shaft. Finally, the sixth natural mode, shown in Figure 5(f), exhibits in-phase rotations of gears that are added to vertical translation in opposite directions leading to a large x_r. Both fifth and sixth natural modes are characterized by negligible horizontal translations. As underlined in Refs. [24, 30], the last natural mode is generally the one responsible for major resonant behavior of spur gears, because it can take place inside a frequency range usually swept by the first harmonic of mesh frequency. Despite this, considering that gear pumps typically have a small number of teeth (usually 7 to 14), small dimensions and an aspect ratio, $b/2R$, that is close to one, the last natural mode is ordinar-

Table 2: Natural frequencies predicted by the dynamic model for the designed gear pump.

Natural mode	Natural frequency
#1	416Hz
#2	357Hz
#3	1278Hz
#4	1844Hz
#5	2960Hz
#6	13948Hz

ily above the frequency range swept by excitations. For the examples pump with $k_{xx}/k_m = 0.1$, natural frequencies corresponding to the first five mode shapes of Figure 5 are 416, 357, 1278, 1844 and 2960 Hz , the sixth natural frequency is 13948 Hz. Moreover, the last natural frequency tends to increase by decreasing the pump displacement, if $b/2R$ is kept as constant.

2.4.2 *Applications and numerical results*

By applying the analytical procedure for variable pressure load estimation described in subsection 2.3 and assuming that the arc length of the pressurizing zone is equal to twice the pitch on the tip circle, the periodic pressure force and torque shown in Figure 6 are obtained. It is worth noting that depending on pressure difference between inlet and outlet, both force and torque show different amplitude and mean value being linearly linked to the outlet pressure. The pressure loads shown in Figure 6 have been used to solve the 6 DOF dynamic system. In order to assess the accuracy of the proposed estimation method, the results are compared to those provided by a high-fidelity model proposed in [3], which is supported by experimental comparison, at working speed of $2000rpm$, as shown in Figure 7. Results obtained from the model in [3] are obtained by simulating the pressure course around gears with a lumped parameters CFD code and then integrating it with respect to the gears geometry. It is worth noting that, despite the presence of some discrepancies related to high order harmonics, the waveform is well represented by the proposed analytical method. The reason is given by the fact that the typical drop

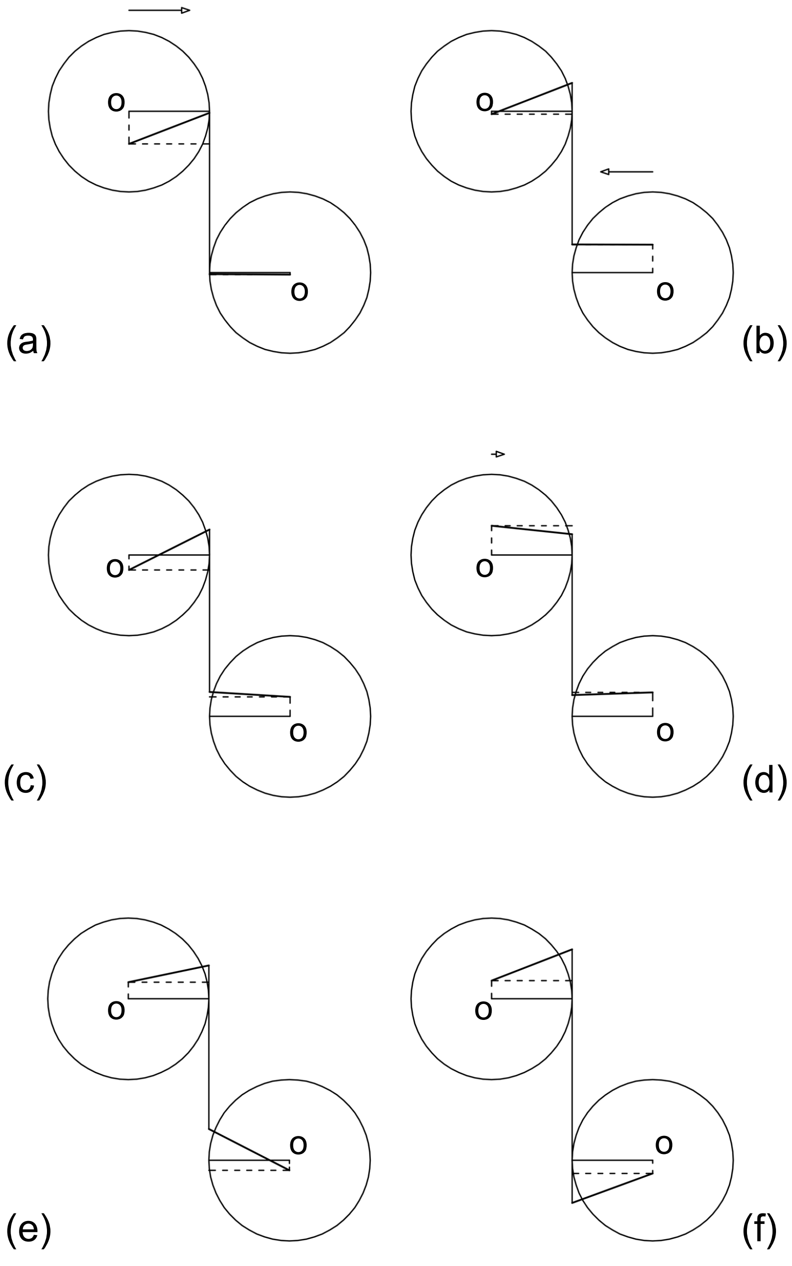

Figure 5: Natural modes of six coupled motions.

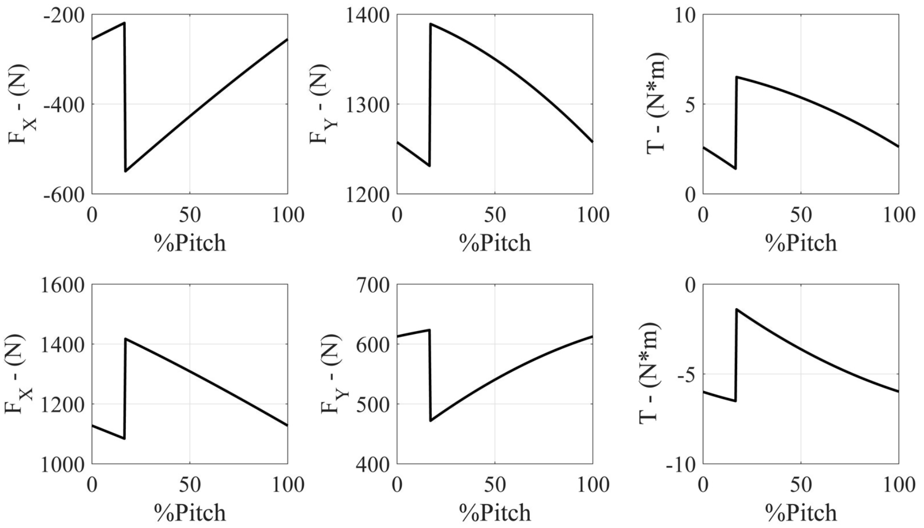

Figure 6: Pressure force and torque calculated assuming absence of high pressure peaks inside the trapped volume and $Pout = 20bar$.

(or sudden increase) shown by such force and torque components, when there are no considerable trapping phenomena, is mainly governed by the pressure difference between inlet and outlet chambers. In order to carry out the analysis, parameter c in Eqn. 16 has been determined experimentally by following the procedure described in subsection 2.3. The experimental campaign has been conducted on 20 nominally identical pumps, with similar main design parameters as the one reported in Table 1; each gear pump has been tested at five different operating speeds, while delivery pressure and oil temperatures were kept as constant. Table 3 shows the five different working conditions used to determine parameter c; results obtained from the experimental campaign are reported in Figure 8, together with the estimation of parameter c based on Eqn. 18 which has been used to solve the dynamic system.

Figure 9 plots the RMS value of the meshing force calculated by using the first five harmonic amplitudes of the response at four different outlet pressures in the absence of high pressure phenomena in the trapped volume. As

Table 3: Test conditions adopted for the estimation of the speed dependent drag torque T_d.

Outlet pressure (bar)	**Oil temperature (°C)**	**Working speed (rpm)**
30	120	500
		1000
		2000
		4000
		6000

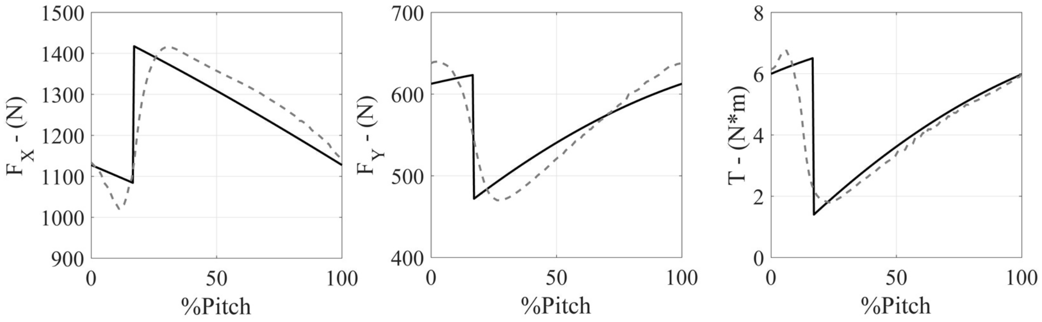

Figure 7: Comparison between pressure force and torque calculated by applying the method in Section 2.3 (solid line) and the high accuracy model defined in [3] (dashed line), with $P_{out} = 20bar$ and $n = 2000rpm$.

proposed in ref. [28], RMS calculation is performed by using the following equation:

$$\langle F_m \rangle_{RMS} = \sum_{\nu=1}^{5} A_\nu^2 \tag{22}$$

where A_ν represents the amplitude value of the ν^{th} harmonics of the mesh frequency. Journal bearing damping matrix $\mathbf{C}_b^{(i)}$ has been defined on the basis of the experimental and numerical data reported in Refs. [42, 43] for full circular bearings, by following the same hypotheses adopted to determine $\mathbf{K}_b^{(i)}$

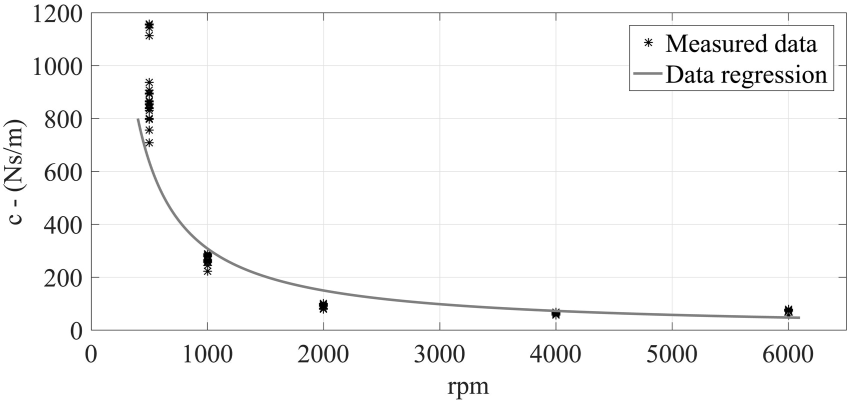

Figure 8: Measured data and statistical regression (with $a_1 = 4092218$, $a_2 = 1.04$, $a_3 = 0$) of friction torque parameter c with respect to the angular speed.

in Eqns. 20 and 21. In particular, as underlined in both Refs. [42, 43], once $\mathbf{K}_b^{(i)}$ has been defined, damping terms are obtained as follows:

$$\mathbf{C}_b^{(1)} = \frac{k_{xx}}{\omega} \begin{bmatrix} 1 & 0.2 \\ 0.2 & 0.08 \end{bmatrix} \tag{23}$$

$$\mathbf{C}_b^{(2)} = \frac{k_{xx}}{\omega} \begin{bmatrix} 1 & -0.2 \\ -0.2 & 0.08 \end{bmatrix} \tag{24}$$

Similarly to Eqns. 20 and 21, matrices defined in Eqns. 23 and 24 refer to the case in which the direction of the applied load coincides with axis x and therefore they must be rotated accordingly if this assumption is not verified.

As expected, the RMS amplitude of the gear mesh force increases with increasing outlet pressure because applied loads are increased both in amplitude and mean value. The dependency between journal bearing damping coefficients and the mean working speed causes the resonance peaks to be asymmetrical. Since the tooth counts of the gears are low, the gear mesh frequency is also low. As such, only the higher harmonics of the excitation excite the natural modes at speeds below 3500 rpm, but RMS amplitudes are kept high due to the damping terms. Above the speed of 3500 rpm, the second and third harmonics of the mesh excitation excite the fifth mode, resulting a

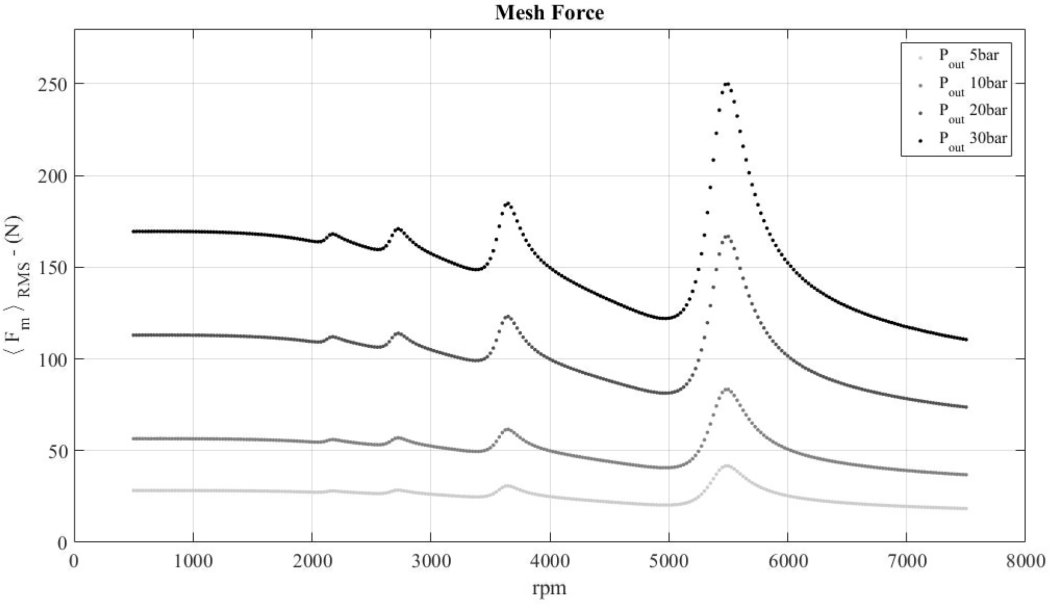

Figure 9: RMS value of the mesh force under four different loading conditions during a speed ramp-up, assuming no overpressure phenomena inside the trapped zone (h=harmonic of the mesh frequency, n_f=natural frequency).

high-amplitude resonance peak. Resonances associated with the others natural modes, with small x_r, are not evident in Figure 9. It is worth underlining that, since mesh stiffness k_m is assumed as a constant, the RMS values of the mesh force and the dynamic transmission error are proportional; for this reason, results are restricted to the analysis of mesh force F_m, which represents a more valuable information regarding the NVH behavior of the pump, from a design-oriented perspective.

The dynamic model concurrently allows the determination of force transmitted to the bearings; following the same procedure adopted to analyze the mesh force, Figure 10 depicts the RMS value of the bearing force along both x and y components, calculated from the amplitude of the first 5 harmonics of mesh frequency for the same parameters as in Figure 9. As it can be observed in Figure 10, the RMS amplitudes of bearing forces is comparable in both directions, showing that a complete analysis of bearing loads must include both components. Bearing force behavior is similar to the behavior of mesh force,

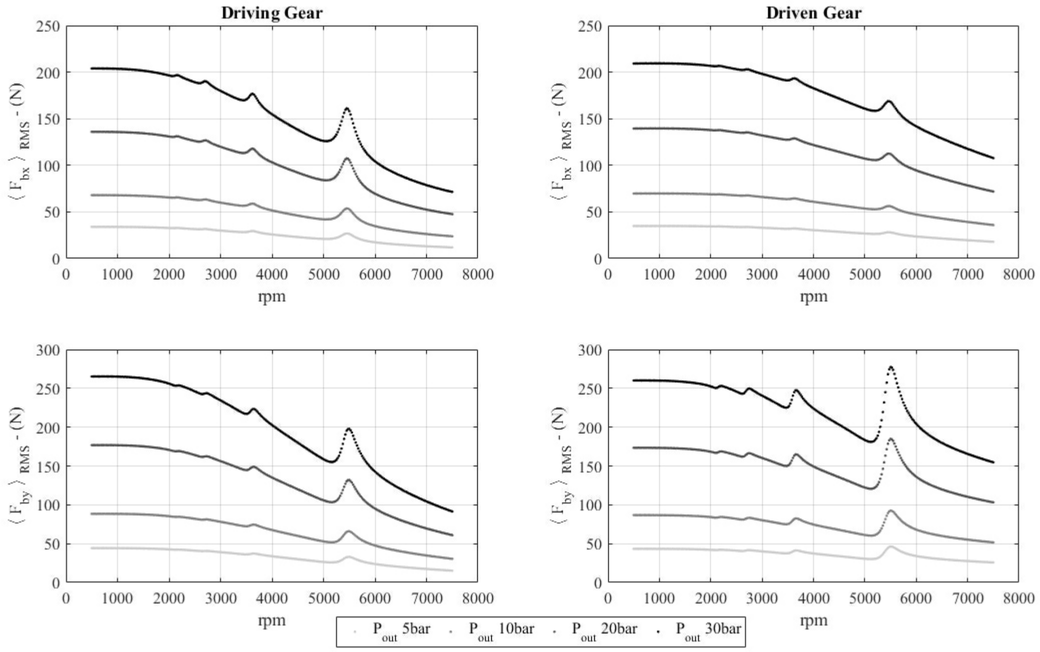

Figure 10: RMS value of the dynamic forces transmitted to the bearings, assuming no overpressure phenomena inside the trapped zone

in particular along the LOA direction, even if the effect produced by the speed increase on the bearing damping terms results to be more evident.

Results shown in Figure 9 and Figure 10 assume that no overpressure phenomena is occurring inside the meshing zone. Despite this being the most desirable condition, gear pumps are often characterized by the presence of high pressure peaks when two tooth pairs are concurrently meshing. As shown in [8] through a wide measurement campaign, depending on the combination between backlash value, relief groove extension and working speed, oil pressure can suddenly rise when the trapping phenomenon takes place. In particular, different relief groove designs can lead to different high-pressure peaks for a given backlash value. Furthermore, a given design characterized by the absence of such high pressure phenomena at a specific working speed can easily exhibit a strong pressure peak in the trapped volume if the speed is increased. These are main concerns for automotive pump applications where smooth operation within a wide speed range is basic requirement, even with an engine as the driver. Therefore, in order to correctly evaluate the pump dynamics throughout the entire speed range covered by the IC engine (and in particular above the $3500 \mathrm{rpm}$ limit), effects produced on the pressure force and torque in presence of high pressure peaks need to be taken into account. For this reason, pressure P_{trap} is assumed to be defined by a quadratic law depending on the angular position of the gears. In particular, when a second tooth pair starts engaging in A (Figure 4), P_{trap} is set as equal to P_{out}. Then it is allowed to increase in a quadratic manner, reaching the maximum value in the middle of the meshing period and going down to the outlet pressure level when the two contact points, respectively, reach points B and D as shown in Figure 4. This variation is given automatically as

$$P_{trap} = 4\left(P_{trap_{max}} - P_{out}\right)\left[-\frac{t^2}{t_{out}^2} + \frac{t}{t_{tot}}\right] \tag{25}$$

where $P_{trap_{max}}$ is the maximum value reached by P_{trap}, t_{tot} represents the time interval in which two pairs in contact, t is the current time instant with respect to t_{tot}.

Results obtained with this method are shown in Figure 11, where the effects of different pressure peaks obtained by increasing the maximum value reached by P_{trap}, namely $P_{trap_{max}}$, are compared. As expected, no differences are detected along the portion of the angular pitch characterized by a single tooth pair engaged. On the contrary, P_{trap} has a significant effect on the amplitude of both pressure force and torque along the remaining portion of the angular pitch. Similar results have been also obtained in [36] from direct measurements of the pressure ripple inside the tooth spaces. On the basis of the results shown in [8], which demonstrates that the maximum value of P_{trap} is linearly dependent on the working speed, three different cases have been analyzed. In particular, for each scenario, P_{trap} is assumed to vary in reference to the angular speed following a different slope. Since the backlash value $\bar{x}_b$, which is defined by design, is kept as a constant, this study is equivalent to analyzing the effect of various relief groove extensions, namely different bridge extensions, on the dynamic behavior of the gear pump. The purpose of the relief groove is to prevent direct contact between the inlet and the outlet chamber through the meshing zone. Theoretically speaking, the extension of such a bridge should be higher, or at least equal, to $p_b * (2 - \varepsilon) * \cos\alpha$, where p_b is the base pitch, ε is the contact ratio and α is the pressure angle. In practice, the quantity $p_b * (2 - \varepsilon) * \cos\alpha$ cannot be reached, otherwise extremely high

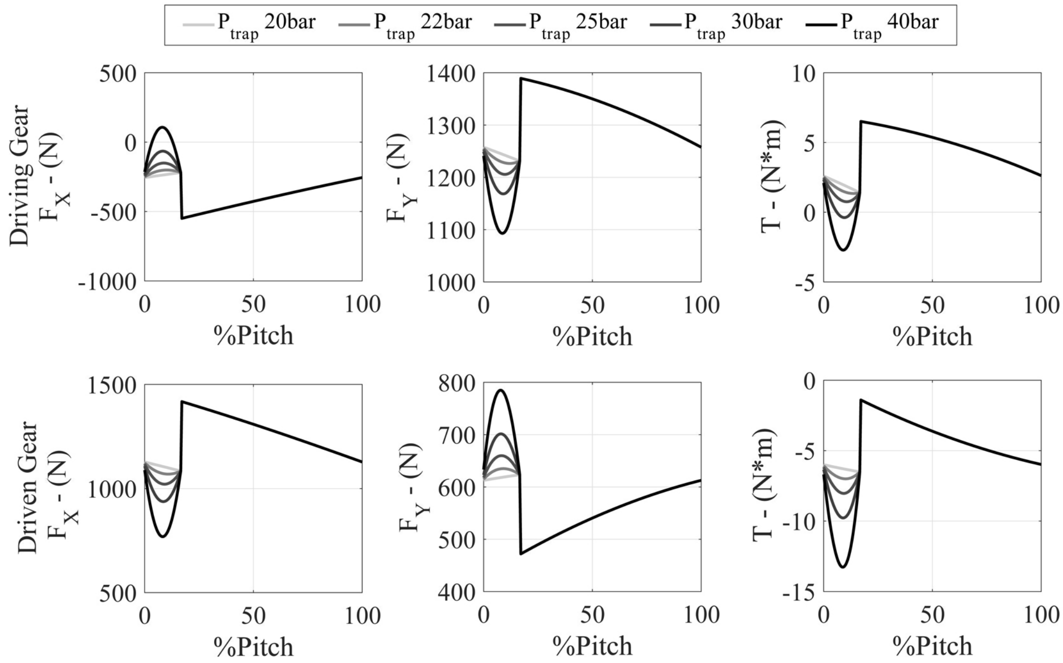

Figure 11: Pressure force and torque in case of $P_{out} = 20bar$ and quadratic overpressure peak inside the trapped volume.

pressure peak phenomena can take place inside the trapped volume causing damages to the gearpair. For this reason, the length of the relief groove is reduced by design of a certain amount; however, in general, the higher is the extension of the relief groove, the higher is the pressure value reached inside the trapped volume [8]. Figure 12 shows the variation of P_{trap} for the three analyzed conditions (namely W, M and T); as underlined in [8], for a given backlash value and angular speed, the wider the relief groove, the higher the maximum value of P_{trap}. In particular, for cases W and M, pressure P_{trap} is assumed to linearly increase with the angular speed throughout the entire speed range while case T is kept as a constant till the angular speed reaches the $2500rpm$ value, when P_{trap} starts rising linearly. As explained in [8], cases W, M and T may be referred to three different extension of the relief groove, from the widest one to the thinnest one respectively.

Figure 13 depicts the RMS value of meshing force calculated from the first 5 mesh frequency harmonics of the response for the cases W, N and T of Figure 12. Here, the results are compared to the $P_{trap} = P_{out}$ condition. Despite the

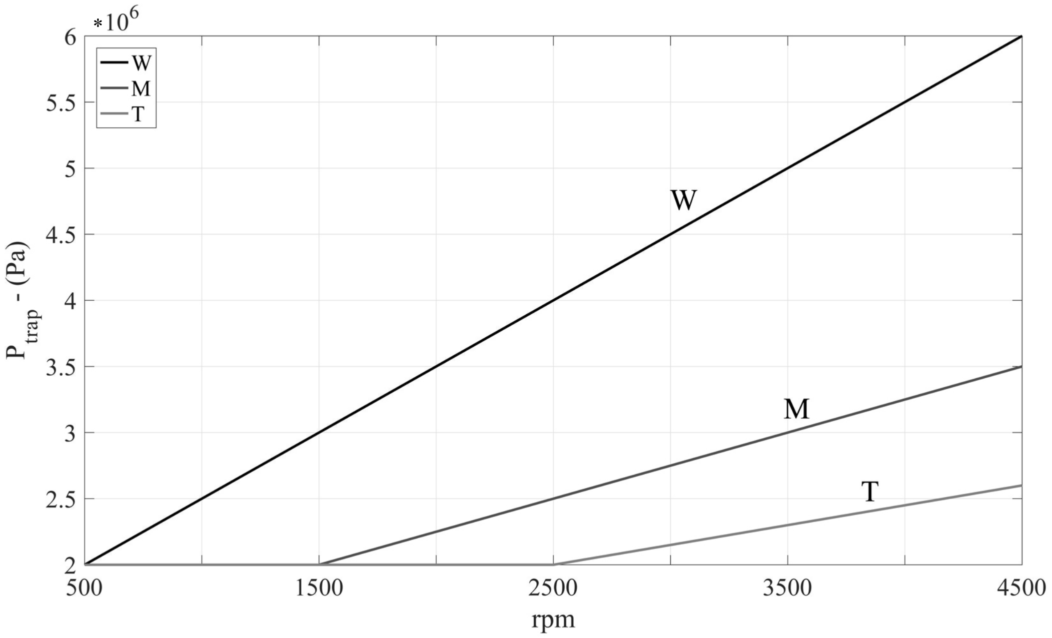

Figure 12: Maximum value of P_{trap} in reference to the working speed, for three different relief groove extensions: $W = wide$, $M = medium$, $T = thin$.

pressure phenomenon in the trapping volume affects a limited fraction of the pressure loads along the angular pitch, it appears to have a deep influence on the dynamic behavior of the gear pair. In particular, meshing force is considerably intensified by high values of P_{trap}, which tends to contrast the bearing damping reduction caused by the speed increase. Similar are also evident in the bearing force amplitudes as plotted in Figure 14, especially along the LOA direction on the bearings supporting the driven gear. On both bearings, along the OLOA direction, the load reaches its maximum values in the speed range between 2500 and 5000 rpm; above this limit, the effect of the speed on the bearing damping terms become predominant and the load is reduced.

Finally, the analysis has been also focused on the effects of the pressurizing zone excitation, which can be controlled, in practice, by designing grooves in the pump's body (for more details, see Ref. Ivantysyn2003, p. 323). Nevertheless, by applying the procedure defined in section 2.3 for estimating variable pressure loads, it is worth noting that the extension of the pressurizing zone only affects the mean components of the pressure forces applied to the gears

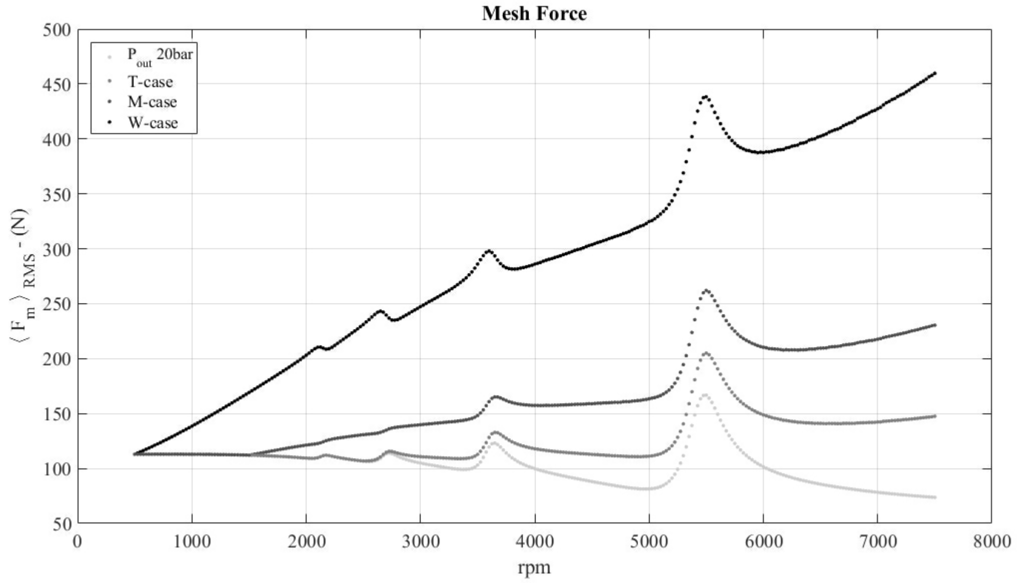

Figure 13: RMS value of the mesh force for the three different P_{trap} cases in comparison to the $P_{trap} = P_{out}$ scenario.

along axes x and y; its harmonic amplitudes, on the contrary, as well as the pressure torque, remains unaltered. For this reason, results show no difference on the dynamic behavior of the gear pair.

2.5 CONCLUDING REMARKS

The Chapter introduces a non-linear dynamic model for studying the effects of different design parameters on the dynamic behavior of gear pumps, focusing attention on a wide working speed interval. The gear pump was modeled by using a 6 degrees of freedom system, taking into account the presence of journal bearings supporting the gear pair. An analytical procedure is presented to calculate variable pressure loads applied to the two gears, in reference to various influencing parameters such as pressurizing zone extension, outlet pressure and potential presence of high pressure phenomena in the trapping volume. Such an approximate analytical approach represents a compulsory choice at the early stage of the design process, since various design parameters (e.g. radial clearances, relief groove shape and dimension) are not

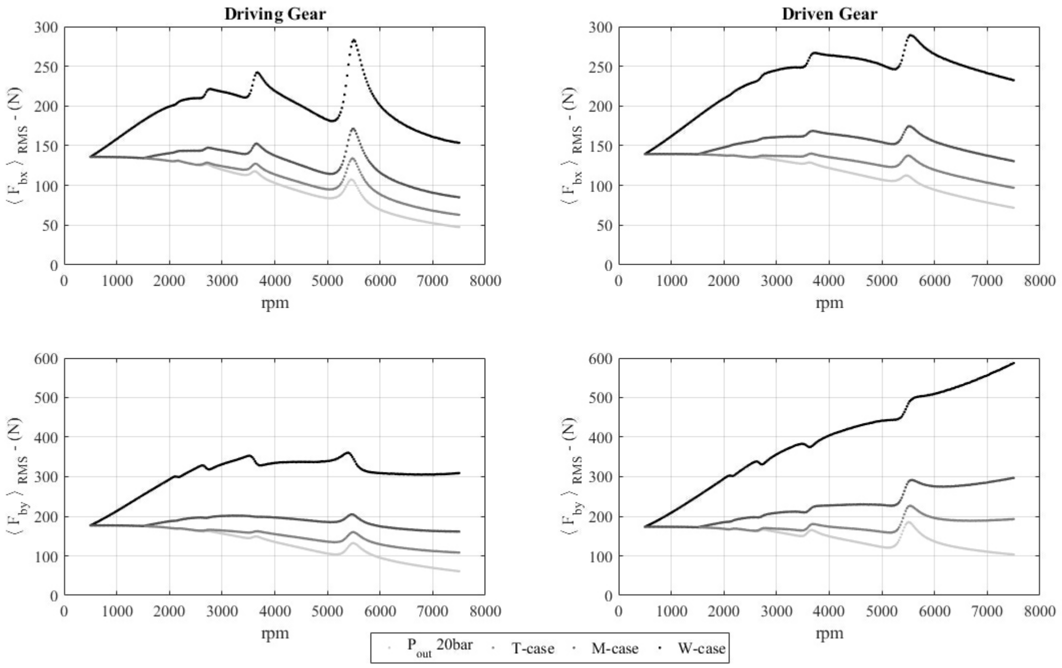

Figure 14: RMS value of the dynamic forces transmitted to the bearings for the three different P_{trap} cases in comparison to the $P_{trap} = P_{out}$ scenario.

already defined. Presence of speed dependent drag torque has been also taken into account. The developed model represents a fast approach to estimate the dynamic behavior of gear pumps based on a limited number of design parameters. These features make it a powerful tool at the early stage of the design process, when the detailed pump geometry is still to be defined. Within this framework, the possibility to estimate the impact of design choices, typically devoted to influence the pump fluid-dynamics on its NVH behavior, improves the efficiency of the design process itself. The originality of the present work stands in the proposed approach itself, which differs from the classical methods that are based on the detailed definition of the entire machine geometry to reach high accuracy results.

A specific spur gear pump has been designed by following basic design rules in order to carry out the analysis. First, the dynamic characteristics of the gear pair have been shown, underlining the presence of four coupled transverse-torsional natural modes; three of them being enclosed in the low frequency range (below 5kHz), while the fourth, which usually has a deep influence on the resonant behavior of gear pairs, is associated with high frequency content (above 10kHz). Since gear pumps are typically characterized by low tooth number (usually between 7 and 14), small global dimensions, and a $b/2r_{ext}$ aspect ratio close to one, the last natural mode is often above the frequency range swept by the excitations.

A parametric study has been conducted in order to evaluate the effects produced by different outlet pressures, presence of speed dependent high-pressure peaks in the trapping volume and various pressurizing zone extensions. Results have shown that the pressure value reached inside the trapping zone has a deep influence on the dynamic behavior of the pump, in particular in the high speed range, where the fifth natural mode can be excited by low order harmonics of mesh frequency. The analysis suggests that careful attention should be paid in the design process of a gear pump working through a wide speed range, since the relief groove must satisfy contrasting requirements. Low speed conditions require an increase of the relief groove width to guarantee high efficiency values, while high speed conditions require to reduce it in order to avoid high pressure phenomena in the trapped volume. Within this context, alternative methods for reducing the high pressure peak inside the trapping volume may become of crucial importance for a better NVH behavior of the pump.

The pressurizing zone extension has been also taken into account during the analysis, showing that different widths of the pressurizing zone lead to different orientations of the pressure force without affecting its amplitude. For this reason, this design characteristic may have a major influence on the static component of the bearing reaction and meshing force, while the dynamic behavior of the pump is not altered.

The results provided by the model underline the presence of deep correlations between the pump NVH characteristics and design aspects typically devoted to improve the pump efficiency and reliability. Further studies should be focused on addressing the concurrent influence of relief groove shape and dimensions, radial clearances and bearings on both the dynamic and fluid-dynamic behavior of these machines.

3

HIGH ACCURACY PREDICTION OF GEAR PUMP PERFORMANCE BY USING LUMPED PARAMETER APPROACHES

The Chapter deals with the description of a methodology to study gear pumps performance by using a lumped parameter approach. The model adopts well-established techniques for simulating the pump fluid-dynamics in association with a novel approach, which allows to take into account the effects produced by the gearpair micromotions. Moreover, possibility to study both spur and helical gears, as well as non-unitary transmission ratio gearpairs has been included, in order to ensure the wide applicability of the model in modern design solutions. Within this framework, a dedicated procedure to estimate variable pressure loads starting from the pressure distribution around gears is presented and compared with two previous techniques described in the literature. The quality of the results provided by the overall model is then addressed by comparing simulated outcomes with measured data obtained from an extended experimental campaign, involving 20 nominally identical samples of the same pump design. Finally, a review of the variety of results provided by the model is given, together with examples of its practical applicability.

3.1 INTRODUCTION

Fluid dynamic performances and dynamic behavior of gear pumps are related each other and strictly connected to several factors, e.g. clearances between components, gear shape, gear meshing, pressure ripple. For this reason, defining empirical correlations between dynamics, fluid-dynamics and design choices would require extremely demanding experimental campaigns, both in terms of time and costs. In order to overcome this practical limitation, starting from the 80s, numerical models based on Lumped Parameter (LP) approaches have been proposed to study performance of gear pumps by focusing the attention on the pressure distribution around the gears and the outlet pressure ripple [44, 45, 46]. These methodologies have been developed further to obtain a more accurate definition of the phenomena inside the meshing zone [15, 47]. Lately, such numerical approaches have been improved with the aim to take into account various physical aspects such as instantaneous positions of gears [35], presence of cavitation [48, 49], use of helical gears and tandem pump configurations [3]. Eaton et al. [9] focused the attention on the pressure inside the trapping volume, with particular reference to aero-engine fuel pumps, underlining the lack of investigations on high-speed working conditions. Concurrently, other studies have been focused on lubrication phenomena [50, 51] and gear balancing, in reference to the presence of journal bearings and lateral bearing blocks [52, 53, 54, 55, 56].

The use of CFD analysis for studying fluid dynamic phenomena in gear pumps is also present in the literature, even if most of the works are limited to 2D simulations. Castilla et al. [57] studied turbulence structure in the suction chamber of an external gear pump, putting into light pros and cons of CFD simulations applied to these machines. Del Campo et al. [58] used a simplified 2D CFD approach for studying the effect of cavitation in the volumetric efficiency of external gear pumps. In these cases, the 2D strategy allows the comprehension of the major fluid dynamic phenomena involved in volumetric devices. Only recently, full 3D simulation has begun to be used for gear pump analysis. Castilla et al. [59] proposed a method to study the fluid flow inside an external gear pump by means of a complete three-dimensional (3D). In a very recent paper, a CFD three-dimensional simulation of an external gear pump was carried out by Yoon et al. [60] in order to investigate the effects of geometrical design parameters on the flow rate, by including the effect of the lateral gap. They determine the most significant factors affecting the pump performance by means of CFD results and analyze the characteristics of the flow field pattern. The main drawback of this numerical approach relies in the high computational effort required to study the variable pressure phenomena in gear pumps for a complete wheel rotation. An extended review of the modeling approaches for efficiency estimation of volumetric machines has been recently carried out by Rundo in [61].

Research has been also focused on describing the pump theoretical characteristics on the basis of purely analytical approaches. One of the first works on this topic pertains to Bonacini [7], who proposed a method to calculate the pump theoretical displacement and discussed the relevance of the bridge design with respect to the flow ripple amplitude. In the same period, Ichikawa et al. [62] discussed the pump flow rate fluctuations in the frequency domain, by relating them to the dynamics of the pipeline. More recently, Manring et al. [41] has extended the approach to gear pump with non-unitary transmission ratio, underlining the theoretical benefits guaranteed by pump designs with $\tau > 1$. Huang et al. in [63] adopted a similar procedure to evaluate the importance of the relief groove design and analyzed the effects produced by gears module and pressure angle on the theoretical delivery flow rate characteristics. An interesting formulation has been finally introduced by Devendran et al. in [64, 65], where the authors proposed a novel formulation for estimating the pump theoretical displacement taking into account the potential adoption of gears with non-symmetric teeth. The work has enlightened the positive potential features of this uncommon design choice.

As it can be appreciated from this literature survey both LP and CFD models can be adopted to evaluate gear pump pressure and flow rate characteristics; each approach has different pros and cons, which make it suitable to be applied during a different step of the design procedure. Purely analytical dissertations, on the contrary, may give important information referring to the theoretical characteristics of the machine, but they cannot be adopted to evaluate the pump behavior in working condition. For this reason, purely analytical methods are usually adopted as constraints in the gearpair design procedure that take place at the very first stages of the design process. CFD approaches may represent the opposite option, since they are based on a very limited number of hypotheses and should allow for a highly detailed modeling of the pump. Unfortunately, such methods require a considerable computational effort and therefore their practical adoption is still not so widespread or restricted to simplified pump geometries. In the field of gear pumps, LP models still represent an efficient and profitable solution, also because the research in the last two decades has brought to the development of accurate software, requiring a reduced computational effort with respect to the obtained estimation accuracy.

Within this framework, the present Chapter describes the mathematical formulation and the practical implementation of a novel LP model for predicting pump efficiency as well as pressure phenomena in gear pumps. The present approach is focused on evaluating the effects of slight design modifications, by taking into account a wide range of design specifications. Moreover, the LP model is coupled with equations of motion of the gearpair, allowing for the calculation of the gears micromotions as a result of the instantaneous balancing between the simultaneous presence of variable pressure loads, a speed dependent drag torque, the meshing force and the bearing reaction. This modeling approach has been firstly introduced by Mucchi et al. [17, 18], but the described model calculates a Stationary Equilibrium Position (SEP) at each angular pitch. Lately, the approach has been revisited by Vacca et al. in [35] by proposing a solution flowchart which allows to calculate the SEP at each frame of calculus; however, the proposed procedure seems not to take into account the effect of the drag torque. Moreover, a clear description of the way adopted to calculate the mesh force is not provided. In order to overcome these limitations, the present model defines a method to estimate the mesh force with respect to the working conditions of the pump, by including also the presence of non-zero drag torque components.

The model introduced hereinafter is also able to include the presence of helical gears, as well as gearpairs with non-unitary transmission ratio and arbitrary shaped relief/lateral grooves. Discharge coefficients, that are usually taken from ref. [14] and then slightly adjusted to reach a better experimental validation (see for example ref. [15]), have been determined with the help of CFD analysis. As stated in Chapter 1, the need to improve the NVH behavior of gear pumps has led to spread the use of helical gear pumps, mostly where low levels of pressure difference and high flow rates are required, even if, in the literature, this kind of gear pump has been rarely studied. The first works on helical gear pumps date back to the forties and they were focused on giving some slight details on the instantaneous and mean flow rate [66, 67]. Later, in [13] the author provided an exhaustive explanation on the way the helix affects the theoretical outlet flow ripple. More recently, in [19] the pressure force and torque acting on helical gears has been discussed, nevertheless, the adopted approach is based on simplified hypothesis that led the authors to neglect components related to the presence of the helix, i.e. the axial pressure force and relative torque components. The application of the numerical methods discussed above has been extended to helical gears just in the more recent literature by Battarra et al. in [2].

Assessment of simulated results obtained from the proposed modeling approach is presented and discussed in the Chapter by comparing them with experimental results. Measured data have been recorded by conducting a dedicated experimental campaign, involving tests on 20 nominally identical samples of a gear pump with helical teeth and nonunitary transmission ratio. Each sample has been geometrically characterized by measuring the mean actual radial and bearing clearances on both gears and then tested at 16 different working points. The comparison shows that the proposed model can guarantee high accuracy predictions in terms of pump volumetric efficiency throughout the entire range of working conditions considered. Concurrently, model sensitivity to slight design modifications is comparable to the real pump behavior.

The following Section proposes the mathematical model adopted to calculate the pressure distribution around the gears, together with the CFD approach adopted to set up discharge coefficients. Section 3.3 regards the mathematical model for calculating gearpair radial movements that has been coupled to the LP fluid dynamic model, while Section 3.6 describes the whole model structure together with its iterative solving workflow. Sections 3.4 and 3.5 contain the description of the analytical procedure built up for the accurate determination of the variable pressure force and torque loading spur and helical gears, respectively. Comments on the estimation quality provided by such procedures are given in both Sections. Sections 3.7 and 3.8 concern the experimental campaign and the assessment of the simulation results, respectively. Finally, last Section is devoted to concluding remarks.

3.2 GEAR PUMPS LUMPED PARAMETER MODELING

Description of the mathematical approach used to determine the pressure variation around gear pumps for a complete gear rotation is given, focusing the attention on the several flow rates determined. The LP approach has been adopted to evaluate the performances of the pump in terms of outlet mass flow rate, outlet pressure ripple, oil pressure evolution during a complete gear rotation and instantaneous volumetric efficiency. Concurrently, in order to improve the LP model results accuracy, a 2D and two 3D CFD models have been developed (see Subsection 3.2.1).

The entire pump and the relative outlet piping system are discretized with a constant number of control volumes, in which all the fluid properties are considered as a constant. Several authors [45, 68, 35, 17] have already applied a similar approach, each of them proposing a different subdivision of the pump volumes, in particular in the meshing zone. In the present model, the discretization of the meshing zone proposed by Vacca et al. in [35] has been implemented, but a different physical approach has been followed. In particular, starting from the Continuity Equation where flow rates are defined in reference to the pressure difference between two control volumes:

$$\frac{dP}{dt} = \frac{B}{V_i}\left[\sum Q_i^{in} - \sum Q_i^{out} - \left(\frac{dV_i}{dt} - \frac{dV_i^{var}}{dt}\right)\right] \tag{26}$$

By assuming a constant angular velocity ω_1 for the driving gear, the Continuity Equation for each control volume referring to that gear can be expressed as:

$$\frac{dP}{d\vartheta_1} = \frac{B}{V_i}\left[\frac{1}{\omega_1}\left(\sum Q_i^{in} - \sum Q_i^{out}\right) - \left(\frac{dV_i}{d\vartheta_1} - \frac{dV_i^{var}}{d\vartheta_1}\right)\right] \tag{27}$$

Similarly, for the driven gear:

$$\frac{dP}{d\vartheta_2} = \frac{B}{V_j}\left[\frac{1}{\omega_2}\left(\sum Q_j^{in} - \sum Q_j^{out}\right) - \left(\frac{dV_j}{d\vartheta_2} - \frac{dV_j^{var}}{d\vartheta_2}\right)\right] \tag{28}$$

Now, by assuming a constant transmission ratio τ, Eqn. 28 can be defined with respect to ϑ_1 as well:

$$\frac{dP}{d\vartheta_1} = \frac{B}{V_j}\left[\frac{1}{\omega_1}\left(\sum Q_j^{in} - \sum Q_j^{out}\right) - \left(\frac{dV_j}{d\vartheta_1} - \frac{dV_j^{var}}{d\vartheta_1}\right)\right] \tag{29}$$

It is therefore clear that, independently from the transmission ratio, all the control volumes can be solved with respect to the instantaneous angular position of the driving gear. Moreover, the choice to work in the angular domain provides a consistent simplification of the model implementation; all the variable geometrical parameters, e.g. volumes V_i and V_j, porting areas, etc. can be calculated and stored at a fixed angular step and then recalled during simulations without the need of further interpolations.

Flow rates connecting control volumes can be defined on the basis of two different approaches. In the hypothesis of low Reynolds numbers #Re, the Couette-Poiseuille equation may be a satisfactory representation of the phenomenon:

$$Q = \frac{wh^3}{12\mu}\frac{\Delta P}{L} + \frac{whu}{2} \tag{30}$$

where u represents the tangential velocity, while w, h and L are the channel width, height and length, respectively. On the other hand, when the hypothesis of low Reynolds numbers does not match the actual flow conditions, flow rates may be defined with the help of the discharge coefficients C_d, by using Eqn. 31, which is obtained from the application of the Bernoulli's equation under specific hypotheses:

$$Q = C_d A \sqrt{\frac{2\left|\Delta P\right|}{\rho}}\, sign\left(\Delta P\right) \tag{31}$$

where A represents the porting area between two control volumes. According to the different links between flow and pressure drop defined by Eqs. 30 and 31, it is important to correctly characterize the several flows describing the interconnections between volumes. This classification is typically performed on the basis of experience and trial and error processes, since, *a priori*, no objective information is available regarding the nature of the various flow rates exchanged between control volumes. However, in the specific field of gear pumps modeling, flow rates are classified in reference to the clearance sizes and the angular position of the reference control volume.

In order to better understand this statement, it is possible to focus the attention of Figure 15, depicting three adjacent tooth pockets moving from the pressurizing zone, where no lateral grooves are present, towards the outlet zone. Inside this region, teeth are surrounded by the casing and the thrust-plate, hence the oil can flow through small channels between tooth tips and casing (giving birth to tooth tip flow rates Q_t), as well as between tooth lateral flanks and thrust-plate/casing (giving birth to tooth lateral flank flow rates Q_f). Since within this zone clearances between case and teeth are designed to provide sealing between high and low pressure sides, leakage is limited as much as possible. The depicted framework allows to fairly assume low #Re flow rates exchanged between consecutive pockets and therefore Eqn.

30 is adopted. The eventual presence of lateral/tip grooves, on the contrary, leads to a completely different scenario. As a matter of fact, such grooves are designed to reduce the angular extension of the pressurizing zone by consistently increasing the radial and axial clearance values at some pre-defined angular sectors of the gearpair. In particular, the amount of clearance is usually so high that it is reasonable to assume all pockets inside this region have the same mean pressure value. As a direct consequence, pockets inside this region do not have significant mutual interactions and flow rates are so small that #Re remains small even if the characteristic linear dimension of the equivalent channel increases considerably. In the present model, the definition of these flows has been conducted analyzing the results of the CFD models that will be introduced and discussed in Subsection 3.2.1. By considering several cases with different clearance values, the flows in the clearance between tooth tip and casing, tooth lateral flank and thrust-plate and tooth lateral flank and casing resulted to be well represented by using Eqn. 30.

By focusing the attention on the meshing zone, the aim is now to describe the discretization scheme adopted to model flow rates exchanged between driving/driven gears and inlet/outlet chambers. Figure 16 shows four consecutive instants of meshing. In Figure 16.a control volume V_i is directly connected to the outlet chamber $\left(Q^i_{outlet}\right)$ and the driven gear pocket V_j; therefore, two different volumetric flow rates have been defined. In this initial part of the meshing course, volume V_{var} is added to the volume of the outlet chamber. In Figure 16.b, control volume V_i does not communicate with the outlet volume; the two teeth are not yet in contact, so tooth space V_i can communicate with two adjacent driven gear pockets: V_j, through flow rate Q^{ij}_m, and V_{j-1}, through flow rate Q^{ij-1}_m. The lack of direct connections with the inlet/outlet chamber causes the absence of term V_{var}. In Figure 16.c, the hydraulic connection between the backflank of the teeth only occurs, therefore the driving gear pocket communicates only with the meshing tooth space of the driven gear, defining the so-called trapping volume. Finally, in Figure 16.d the meshing is ending and control volume V_i communicates directly with the inlet $\left(Q^i_{inlet}\right)$; in this final part of the meshing course, volume V_{var} is added to the volume of the inlet chamber. Therefore, depending on the actual meshing condition, four different flows can be detected, as well as a new shape of the control volume. Indeed, during the meshing evolution, as proposed in [35], the shape of the control volume is conventionally limited by the minimum distance between

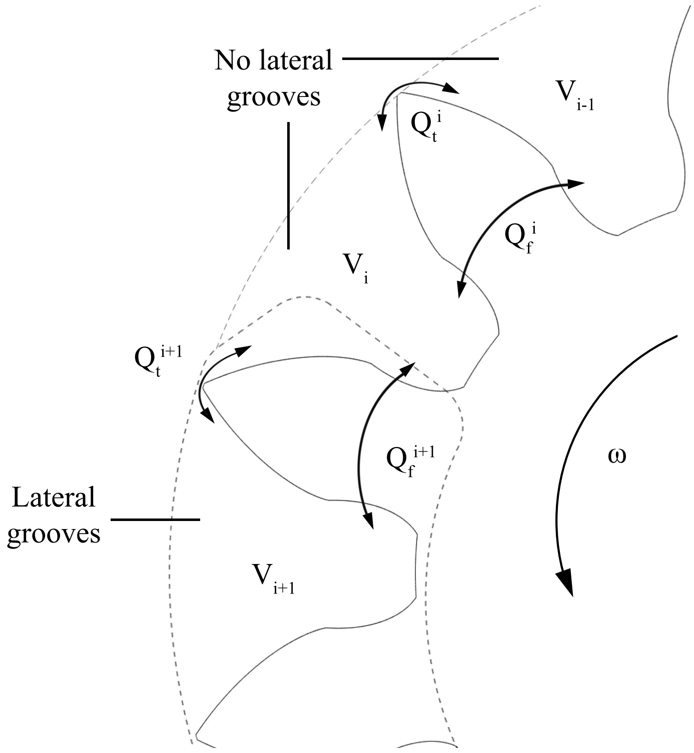

Figure 15: Flow rates between adjacent tooth pockets inside the pressurizing zone, in both regions with lateral grooves and without lateral grooves.

the flanks of two meshing teeth. Consequently, the minimum distance is also used to define such flow rates. Additional details regarding the discretization procedure adopted in the meshing zone may be found in [35] - Section 2.1, in which the presence of volume discontinuities and variable volumes is discussed.

3.2.1 *CFD analysis*

The description of the mathematical model in Section 3.2 has enlightened the necessity to infer, predict or, at least, reasonably assume the nature of each flow rate exchanged between control volumes. In order to improve the comprehension of the flow behavior within the micro-scale gaps, two-dimensional and three-dimensional CFD models have been developed. These models have been used with the aim of investigating some specific fluid dynamics phe-

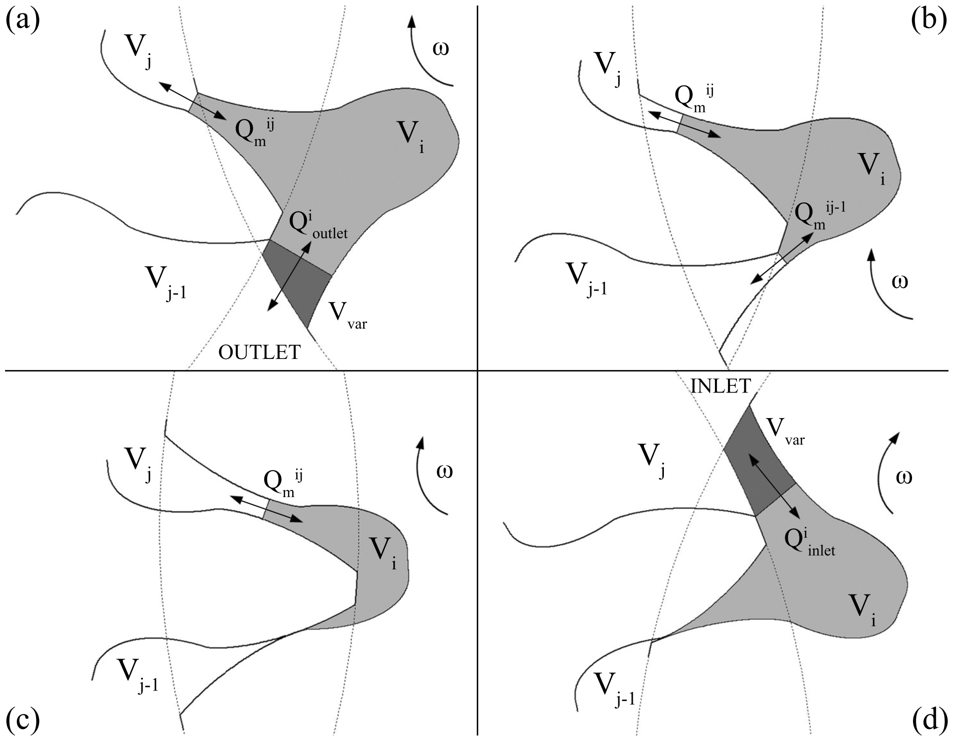

Figure 16: Mutual flow connections between meshing pockets, together with inlet and outlet chambers.

nomena that occur in these fluid zones characterized by very small passage areas. Since the computational efforts could represent an obstacle in the investigation of the fully developed pump geometry, the CFD analysis refers to particular areas of the pump and allows the calculation of flow discharge coefficients in order to better reproduce the actual flow behavior inside the gear pump during the solution of the lumped parameter model. In the light of this purpose, the following considerations arise.

(i) Each numerical simulation refers to a single gear position in stationary condition and with wall motion not included; thus, since the resulting flow coefficients become not influenced by the rotational speed of the pump, a more general characterization of the flow condition in a definite number of instantaneous geometrical pump configurations can be obtained. The adherence condition on the moving wall would imply the modification of the velocity profile, and in turn, the variation of the total mass flow rate across the gap. This fact, would reduce the possibility to adopt the C_d value obtained for a specific wall velocity (representative of a single pump operating point), to the same geometry with a different wall velocity (different pump operating point).

(ii) Suitable turbulence boundary conditions were set for each numerical domain. Small gaps, high fluid viscosity and high peripheral velocity makes the flow regime difficult to be *a priori* estimated. A sensitivity analysis on the effect of the turbulence model demonstrated the robustness of the simulations, also when the local Reynolds number falls below classical turbulence transition regions. All the numerical simulations were carried out by means of ANSYS Fluent 13.0. Second order upwind was used as advection scheme for the momentum equation. Pressure based solver and SIMPLE scheme were also adopted.

3.2.1.1 *Turbulence model and grid sensitivity analysis*

In order to setup the most appropriate CFD numerical model, a preliminary sensitivity analysis regarding turbulence model and the number of elements in the gap is carried out. Laminar flow (i.e. no turbulence model activated), k-Epsilon model with standard wall function and k-Omega model were tested against a variable number of triangular elements from 2 to 15. The two-dimensional domain used for this analysis, refers to a tooth-tip gap equal to $10\mu m$ and a pressure difference of $2 bar$. More details about the computational domain are reported in the next paragraph. In Figure 17.a two mesh grids are reported corresponding to a tooth-tip gap discretization with 2 and 9 elements. The results of the sensitivity analysis are depicted in Figure 17.b. The average values of flow velocity in correspondence of the tooth-tip gap are reported against the number of elements. As it can be seen from Figure 17.b, the k-Omega model trend well matches the laminar flow trend with a difference less than 0.7% (the maximum difference refers to the case with 2 elements). On the contrary, the k-Espilon model shows a maximum variation of 3.1% with respect to the laminar flow case. Since the k-Omega model has demonstrated to be able to well represent the flow field also in the case of transition/laminar condition [69, 70] this model was chosen for the CFD analysis.

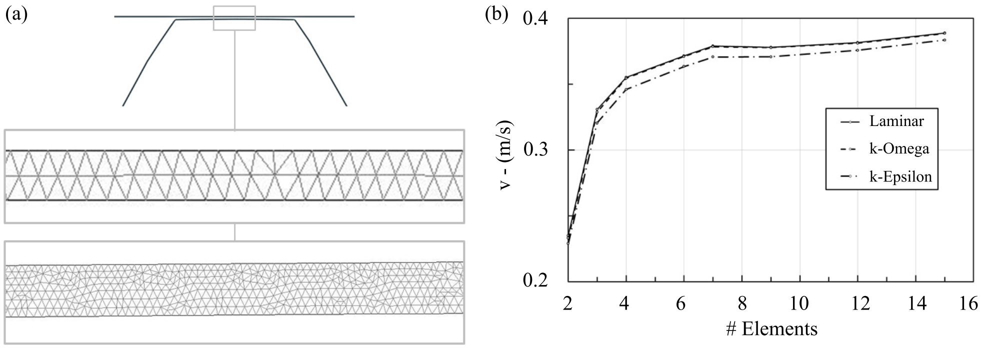

Figure 17: Turbulence model and grid sensitivity analysis: a) meshes with 2 and 9 triangular elements, b) average velocity trends.

3.2.1.2 *Tooth-tip*

The first CFD analysis refers to the clearance between tooth-tip and casing. For each tooth, this clearance changes according to the tooth-wheel angular position due to the eccentricity of the wheels. This is mainly due to the higher pressure in the discharge chamber that forces each wheel towards the suction chamber. Since this clearance varies its value continuously from the minimum value (equal to 5μm) to the maximum value (equal to 130μm), several geometric configurations and pressure conditions are taken into account by using a two-dimensional (2D) CFD approach. The numerical domain is reported in Figure 18, where the tooth-tip/case clearance was modified in reference to the values reported in the Table 4. The pressure boundary condition has been set in order to cover the entire range of pressure difference involved, in the gear pump operation, between two adjacent tooth spaces, which is necessarily smaller than the pressure difference existing between the inlet and outlet chamber of the pump. The pressure conditions used in this analysis are reported in Table 5 and refer to the pressure difference between the starting and the ending sections of the CFD domain (see Figure 18).

Since the number of numerical simulations obtained by the combination of the tooth-tip/casing clearances with the pressure boundary conditions is equal to 154 (i.e. 14 tooth-tip/casing clearance times 11 pressure differences as in Table 4 and Table 5) a two-dimensional (2D) CFD approach was used. The 2D approach allows the reduction of the computational efforts by limiting the reliability of the results, as reported in [71]. In this case, the CFD analysis

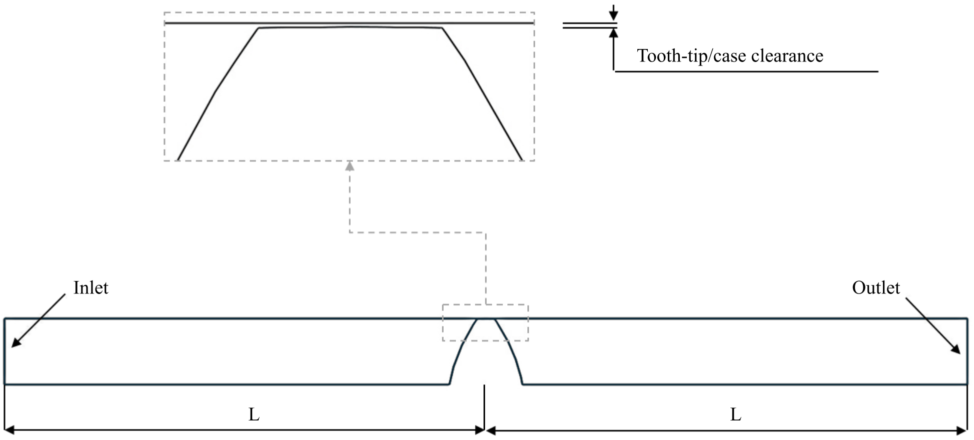

Figure 18: Numerical domain of the tooth-tip/case clearance analysis; the total channel length is equal to 12 times the tooth width on the root circle.

Table 4: Tooth-tip/case clearance values used in the numerical domain defined in Figure 18.

#	**Tooth-tip/case clearance** (μm)	#	**Tooth-tip/case clearance** (μm)
1	5	8	40
2	10	9	60
3	15	10	80
4	20	11	100
5	25	12	120
6	30	13	125
7	35	14	130

Table 5: Pressure differences between the starting and ending sections defined in Figure 18.

ΔP - (bar)										
10	7.5	6.00	5.00	4.30	1.00	0.75	0.60	0.50	0.43	0.02

is devoted to calculate the flow discharge coefficient referred to the tooth-tip gap geometry without considering the presence of the lateral flank clearance. This is consistent with the implementation adopted in the lumped parameter

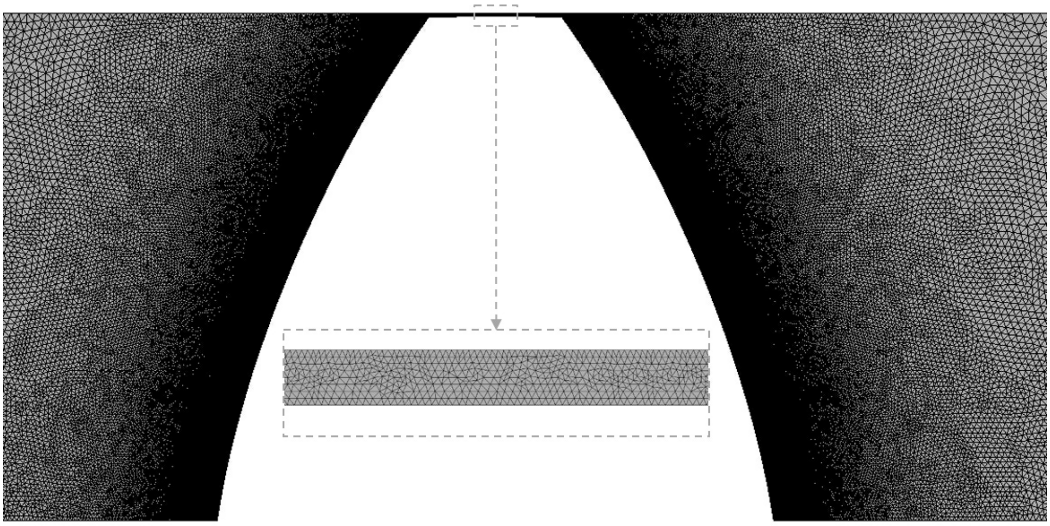

Figure 19: Computational mesh used in the tooth-head/casing analysis.

model, where the tooth-tip flow leakage is uncoupled from the lateral flow leakage and gives more universal meaning to these specific calculations. The numerical domain is reported in Figure 18. The numerical domain is meshed by using triangular elements as reported in Figure 19. In the tooth-tip/case clearance, a minimum of 8 triangular elements are present in order to well represent the velocity profile from the tooth-tip to the case (close-up in Figure 19). Figure 19 reports also the grid refinement close to the tooth that has been adopted in order to generate an uniform distributed mesh, according to the local variation of the velocity magnitude.

3.2.1.3 *Tooth lateral flank*

The second CFD analysis refers to the tooth lateral flank clearance. The lateral clearance is variable along the tooth path. In the inner regions, the lateral clearance is equal to the smallest value (5μm), while in the outer regions, the lateral clearance is equal to 200μm and 500μm as a function of the tooth side (i.e. clearance between tooth lateral flank and case and clearance between tooth lateral flank and cover-plate). The variation of the tooth lateral flank clearance due to the angular position of the wheel corresponds also with the variation of the tooth-tip/case clearance as mentioned above. For this reason, several numerical domains were created in order to combine the tooth lateral flank clearances with the tooth-tip/case clearances. Differently from the previous case, the flow condition in lateral flanks is very dependent from the specific pump geometry and, since they are always present in conjunction with the tooth-tip/case gap, it was decided to include in the numerical domain the concurrent presence of these two gaps.

The CFD models are generated in a similar manner to those realized for the tooth tip/case clearance. Since the lateral clearance is developed along the perpendicular plane with respect to the tooth tip/case, the numerical models refer to a three-dimensional geometry. A representation of the numerical model is reported in Figure 20, where the lateral clearance is highlighted. The numerical model refers to a half of the tooth width and symmetry boundary conditions are imposed in the opposite side of the lateral clearance, as reported in Figure 20. The pressure boundary condition was set in order to cover the entire pressure range involved in the gear pump operation. The pressure conditions (pressure difference between starting and ending sections) used in this second analysis is the same used in the previous one, are reported in Table 5. The numerical domain is meshed by using a hexahedral mesh. In the clearances between tooth tip and case and in tooth lateral flank clearance 11 hexahedral elements are present in order to well represent the velocity (close-up in Figure 20). Moreover, the grid refinement close to the tooth is adopted in order to generate a uniform distributed mesh, according to the local variation of the velocity magnitude. The combinations of the (i) lateral clearance, (ii) tooth-tip/casing clearance and (iii) the pressure condition used in the numerical investigation refer to a typical operating condition of the gear pump. The smallest clearance is characterized by the highest pressure drop across the tooth, while the higher clearances are characterized by the lower pressure drop across the tooth.

3.2.1.4 *Meshing zone*

The last numerical CFD analysis refers to the meshing zone. The meshing zone of the gear pump is characterized by very inhomogeneous flow due to the narrow passage that link the outlet gear pump chamber (high pressure) with the inlet gear pump chamber (low pressure). Conversely, delivery side is characterized by quite uniform pressure field and then very low pressure difference. In this region the lumped parameter model works well by using standard C_d values. In the meshing region at the inlet side, due to the narrow

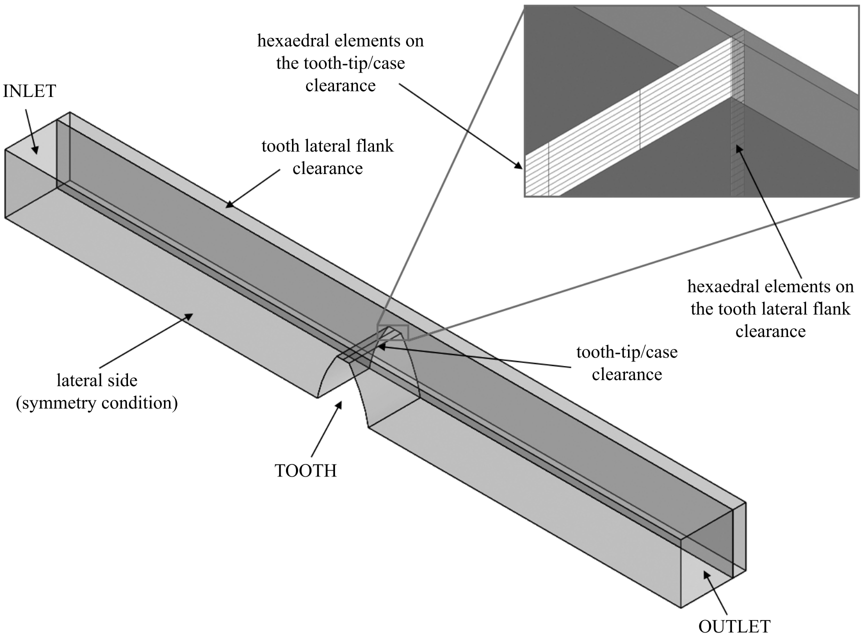

Figure 20: Numerical domain of the lateral tooth flank clearance analysis.

passage and the highest pressure difference, the turbulent eddies grow and monopolize the meshing regions at the inlet side. For all of these reasons, the CFD calculation represents the only method to analyze the flow condition and compute the discharge coefficient for tuning the lumped parameter model. Thus, the CFD analysis will address the inlet side solely.

The CFD numerical model of the meshing zone has to represent the actual subsequently position covered by the driving and driven gears. Figure 21 reports three geometrical configurations considered in the CFD analysis. In order to well discretize the angular position of the gear, each geometric configuration reported in Figure 21 was studied also for other two gearpair positions obtained imposing an angular rotation of the wheel equal to $3 degrees$ forward and $3 degrees$ backward. Therefore, nine CFD numerical domains were performed and studied by using a single pressure difference between the inlet and outlet sections. The pressure difference is directly related to the operating condition of the gear pump, and thus, each configuration is studied for a pressure difference between inlet and outlet equal to $30 bar$.

The CFD numerical model refers to close-up reported in Figure 21. Each configuration has been studied by using only a portion of the meshing zone defined according to the different pressure condition of the inlet and outlet chambers. Figure 22 reports the CFD numerical domain of the third geometrical configuration (see Figure 21.c) with the pressure boundary conditions. Figure 22 allows the comprehension of the meshing region configuration: (i) the lateral tooth region is characterized by the lateral grooves on the cover plate and case and (ii) the two teeth resulting in the meshing region determine the narrow passage characterized by two tooth flanks and by one tooth flank and one tooth tip. Due to these geometrical features of the meshing region, the numerical CFD simulation allows the calculation of four different discharge coefficients: (i) between two tooth flanks, (ii) between tooth tip and the tooth flank, (iii) in the clearance between lateral tooth flank and the case and finally (iv) in the clearance between lateral tooth flank and the cover-plate.

3.3 MATHEMATICAL MODEL FOR ESTIMATING GEARPAIR RADIAL MOVEMENTS

The present Section introduces the modeling procedure defined to calculate gearpair radial movements with respect to the variable loads applied. As stated in Section 2.2 of Chapter 2, the nonlinear equation system describing the dynamics of gear pumps expressed with Eqn. 1 can be rewritten as:

$$\left.\begin{array}{l} m_1\ddot{x}_1 + F_{bx}^{(1)} + F_{px}^{(1)} = 0 \\ m_1\ddot{y}_1 + F_{by}^{(1)} + F_{py}^{(1)} + F_m = 0 \\ J_1\ddot{\theta}_1 + T_{shaft} - r_1 F_m + T_d^{(1)} - T_p^{(1)} = 0 \\ m_2\ddot{x}_2 + F_{bx}^{(2)} + F_{px}^{(2)} = 0 \\ m_2\ddot{y}_2 + F_{by}^{(2)} + F_{py}^{(2)} - F_m = 0 \\ J_2\ddot{\theta}_2 - r_2 F_m + T_d^{(2)} - T_p^{(2)} = 0 \end{array}\right\} \tag{32}$$

where terms $F_{bx}^{(i)}$, $F_{by}^{(i)}$ are the components of the journal bearing's reaction supporting gear i. As proposed in [17], by assuming the inertia terms can

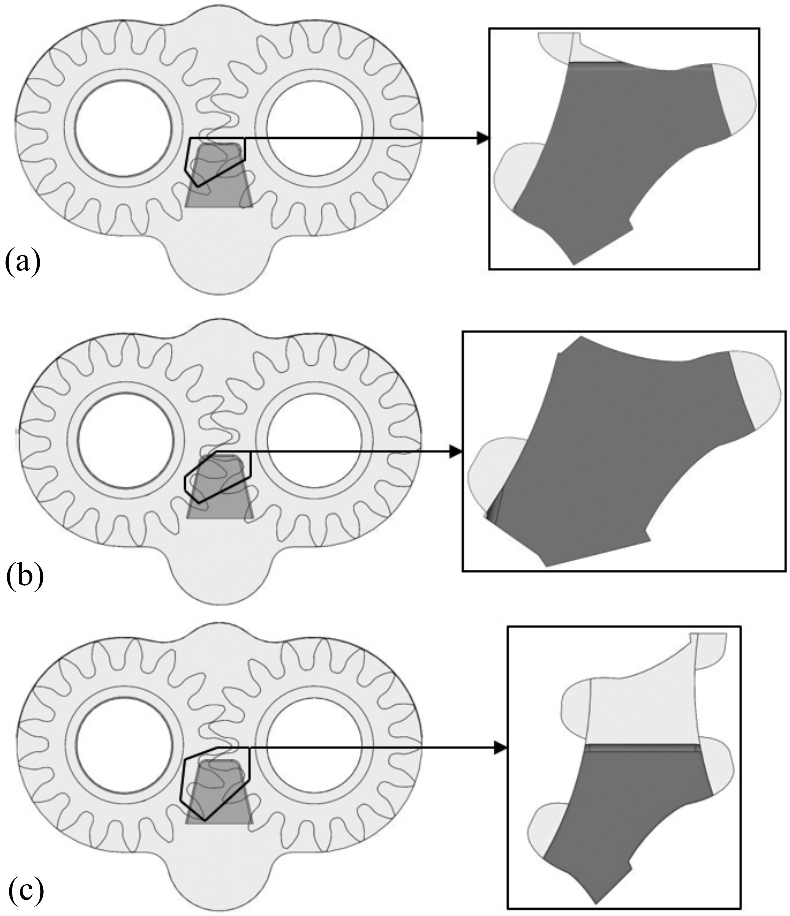

Figure 21: Three numerical domains of the meshing zone analysis.

be neglected, the dynamic system described in Eqn. 32 can be simplified as follows:

$$\left.\begin{aligned}
&F_{bx}^{(1)} + F_{px}^{(1)} = 0\\
&F_{by}^{(1)} + F_{py}^{(1)} + F_m = 0\\
&T_{shaft} - r_1 F_m + T_d^{(1)} - T_p^{(1)} = 0\\
&F_{bx}^{(2)} + F_{px}^{(2)} = 0\\
&F_{by}^{(2)} + F_{py}^{(2)} - F_m = 0\\
&r_2 F_m + T_d^{(2)} - T_p^{(2)} = 0
\end{aligned}\right\} \tag{33}$$

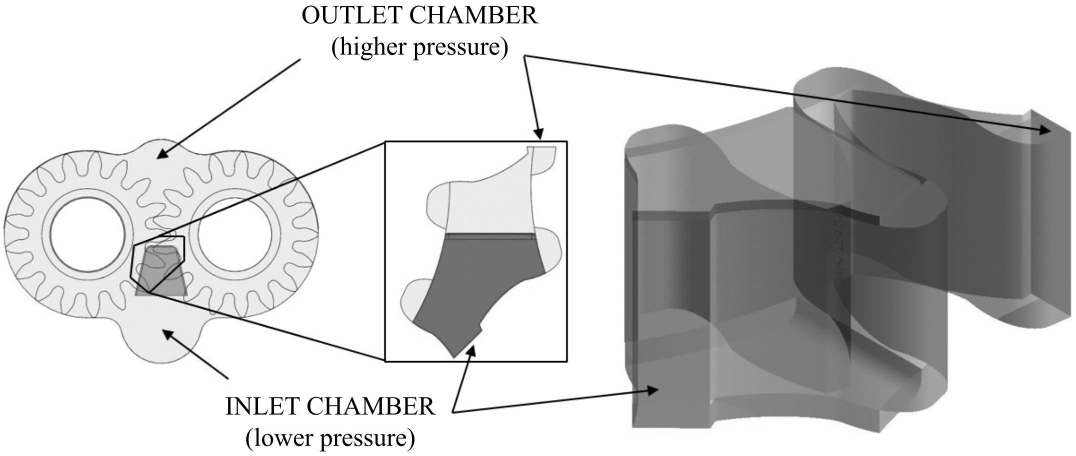

Figure 22: Pressure boundary conditions of the third geometrical configuration (see Figure 21).

where the first two equations describe the radial motion of the driving gear and the fourth and fifth equations describe the radial motion of the driven one. Therefore, the hypothesis adopted in Eqn. 33 reduces the mathematical model describing the gearpair centers position to the $4-DOF$ equation system:

$$\left.\begin{array}{l} F_{bx}^{(1)}+F_{px}^{(1)}=0 \\ F_{by}^{(1)}+F_{py}^{(1)}+F_m=0 \\ F_{bx}^{(2)}+F_{px}^{(2)}=0 \\ F_{by}^{(2)}+F_{py}^{(2)}-F_m=0 \end{array}\right\} \tag{34}$$

which substantially represents the force balance both for contributions along the line of action and normal to it. Moreover, the two equations describing the torque balance on the two gears can be used to estimate the meshing force F_m without necessarily estimate the mesh stiffness and damping coefficients. In particular, starting from the equation system reported hereafter:

$$\left.\begin{array}{l} r_1 F_m = T_{shaft}+T_d^{(1)}-T_p^{(1)} \\ r_2 F_m = T_p^{(2)}-T_d^{(2)} \end{array}\right\} \tag{35}$$

By focusing the attention on the case where driving and driven gear are identical, i.e. $r_1 = r_2 = r$, it is reasonable to assume that $T_d^{(1)} = T_d^{(2)} = T_d$ and the summation term by term between the two equations reported in Eqn. 35 leads to the following expression defining meshing force F_m:

$$F_m = \frac{T_{shaft} + T_p^{(2)} - T_p^{(1)}}{2r} \tag{36}$$

On the contrary, in the case where driving and driven gear are not identical, i.e. in general $r_1 \neq r_2$ and transmission ration $\tau \neq 1$, by subtracting term by term the two equations in Eqn. 35, meshing force F_m is defined as follows:

$$F_m = \frac{T_{shaft} - T_d^{(1)} - T_d^{(2)} - T_p^{(1)} - T_p^{(2)}}{r_1 - r_2} \tag{37}$$

Moreover, taking into account that the total friction torque can be defined with respect to the hydro-mechanical efficiency η_{HM} of the pump:

$$T_d^{tot} = T_d^{(1)} + T_d^{(2)} = T_{shaft}\,(1 - \eta_{HM}) \tag{38}$$

meshing force F_m can be determined without directly calculating the friction terms:

$$F_m = \frac{\eta_{HM} T_{shaft} - T_p^{(1)} - T_p^{(2)}}{r_1 - r_2} \tag{39}$$

It is worth noting that Eqn. 39 does not apply for pumps made by two identical gears since the denominator would be equal to zero.

The presented approach substantially differs from the methodology introduced in [17], as well as the one proposed in [35], since in the present dissertation the estimation of the meshing force takes into account the contribution of the pressure torque applied on both gears together with the contribution of the driving and friction torques. On the contrary, the method proposed in [17] estimates meshing force F_m by assuming the absence of friction and therefore from Eqn. 35:

$$F_m = \frac{-T_p^{(2)}}{r_2} \tag{40}$$

This approach has the quality to require no extra-data regarding the gear pump under study, i.e. hydro-mechanical efficiency η_{HM} and driving torque

T_{shaft}, but it is based on more limiting hypotheses. Concurrently, the method proposed in [35] does not consider the presence of friction torque by assuming $\eta_{HM} = 1$. In the same work, meshing force F_m is assumed as a constant along the entire revolution and no information are provided about its estimation.

Once meshing force F_m has been defined, the determination of the gear center position requires the calculation of the contributions provided by variable pressure loads $F_{px}^{(i)}$, $F_{py}^{(i)}$, $T_p^{(i)}$ and bearing reactions $F_{bx}^{(i)}$ and $F_{by}^{(i)}$. In particular, the formers are directly calculated from the pressure distribution determined by solving the relative lumped parameter model; the analytical procedure followed for their determination will be described in Section 3.4, for the spur gears case, and in Section 3.5, for the helical gear one. Regarding the journal bearing reactions, components $F_{bx}^{(i)}$ and $F_{by}^{(i)}$ are estimated by following the analytical approach described in [72]. The methodology is based on the correction of the formulae obtained under the half Sommerfield conditions for infinitely long/short bearings [73, 74], by means of polynomial correction functions that depend on the bearing aspect ratio L/D. The adopted approach has the benefit to be valid for a wider range of aspect ratio than the solution proposed by Ocvirk in [75] and applied in [35]; concurrently, it is based on simpler expressions with respect to the model proposed by Childs et al. in [76], that has been used in [17].

3.4 PRESSURE FORCE AND TORQUE ESTIMATION IN CASE OF SPUR GEARS

The methodology introduced hereafter can be considered as a complete method to determine the pressure forces and torques in external gear pumps. Figure 23 depicts the reference scheme of the proposed procedure in a generic external gear pump; on the center of each gear, a 3D reference system is located and the pressure forces applied on the two gears are studied separately. Subscript 'p' is neglected along the entire dissertation in Sections 3.4 and 3.5 since all the force components are due to the oil pressure. Let consider the generic tooth space V_i of the driving gear and the two adjacent tooth spaces, namely V_j and V_{j-1}, which share oil flow rates during the meshing course. Along a complete revolution, two different configurations are identified, distinguishing whether the reference tooth space is outside, or inside the meshing zone. It has to be underlined that within such a methodology, the meshing zone starts conventionally when the tooth of the driven gear enters into the cir-

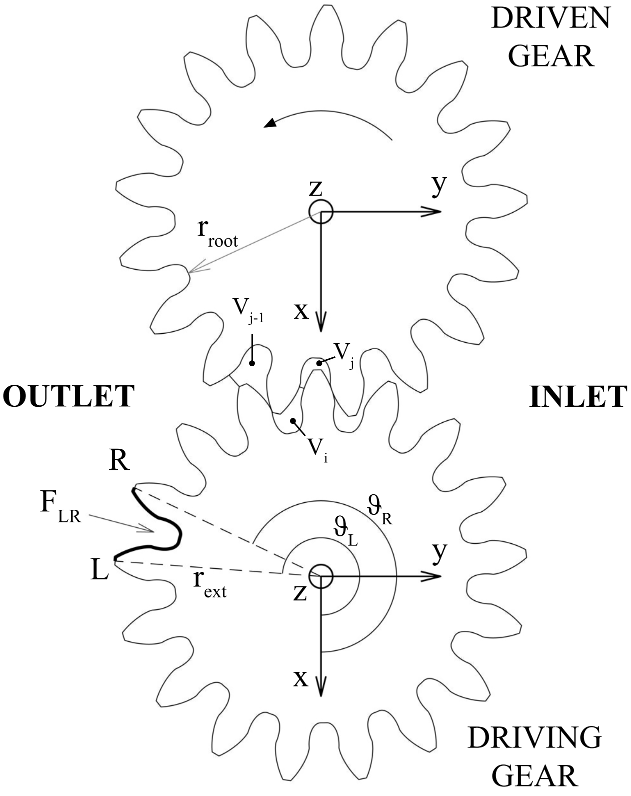

Figure 23: Reference scheme for pressure force determination.

cle defined by radius r_{ext} and not when the real contact occurs; concurrently, it ends when the tooth of the driven gear exits from the same circle and not when the real contact ends. This rule is used to obtain a suitable discretization of the tooth spaces along the meshing course without affecting the accuracy in modeling the meshing process.

3.4.1 *Tooth spaces out of the meshing zone*

Within this layout, the oil pressure acts symmetrically on the entire tooth space surface and, therefore, pressure force F_{LR}, due to the generic tooth space V_i, does not have a tangential component ($F_{LR} = F_{LR,r}$), as it can be seen in

Figure 23. In this frame, F_{LR} can be determined, as described in [17], with Eqn. 41:

$$|F_{LR}| = 2bP_i \sin\left(\frac{\vartheta_L - \vartheta_R}{2}\right) r_{ext} \tag{41}$$

The absence of a tangential component leads to the absence of pressure torque applied to the gear. The line of action of the pressure force applied to tooth pockets outside the meshing area passes through the gear center; therefore such a force, considered applied on the gear center, exhibits the following components along axes x and y, respectively:

$$F^x_{tot,i} = -|F_{LR}| \cos\left(\frac{\vartheta_L + \vartheta_R}{2}\right) \tag{42}$$

$$F^y_{tot,i} = -|F_{LR}| \sin\left(\frac{\vartheta_L + \vartheta_R}{2}\right) \tag{43}$$

Moreover, the tooth spaces layout of a spur gear leads to the absence of pressure force components along axis z $\left(F^z_{tot,i} = 0\right)$.

3.4.2 *Tooth spaces inside the meshing zone*

When tooth space V_i enters within the meshing zone, it is necessary to consider that a different discretization of the control volume is adopted and, in particular, three different control volumes contribute to the definition of the reference tooth space surface (Figure 24). As a result, the pocket is divided into three regions, each one under the loading of a different pressure and separated by contact point K and point of minimum distance H (Figure 25). Points K and H are found and the minimum distance is calculated numerically, by using a specific search algorithm, similarly to the procedures followed in [35, 77]. The calculus procedure starts with the geometrical definition of the teeth inside the meshing zone with two vectors of points. Vector V_1 describes, point by point, the boundary of a tooth of the driving gear, together with its tooth space. Vector V_2 describes, point by point, the boundary of the tooth of the driven gear that is meshing with the former (together with its tooth space). To

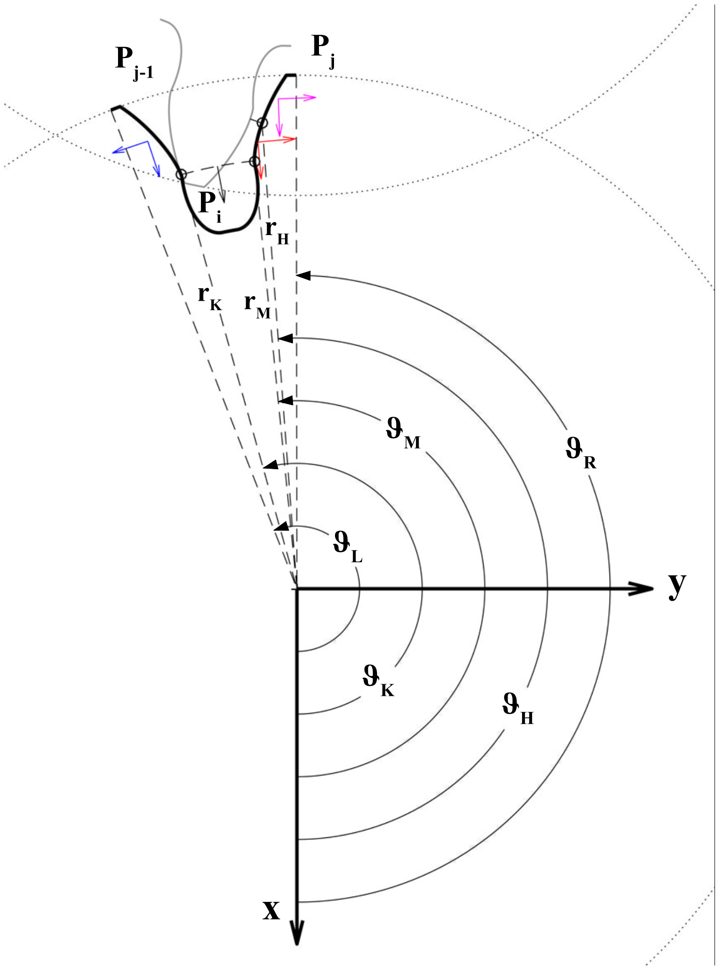

Figure 24: Discretization of the tooth space in the meshing zone.

determine the minimum distance, the algorithm calculates for each point of V_1 the distance from all the points defined in V_2 and then finds the minimum one. Pressure P_i of the reference control volume acts on the central region, while the two external regions are influenced by pressures P_j and P_{j-1}, belonging to control volumes V_j and V_{j-1} previously defined; the three regions are analyzed separately, defining for each one the acting forces (see Figure 25 and Figure 26).

In the region located on the left side of the tooth space, between points L and K, pressure P_{j-1} is acting and the connected pressure force F_{LK} can be

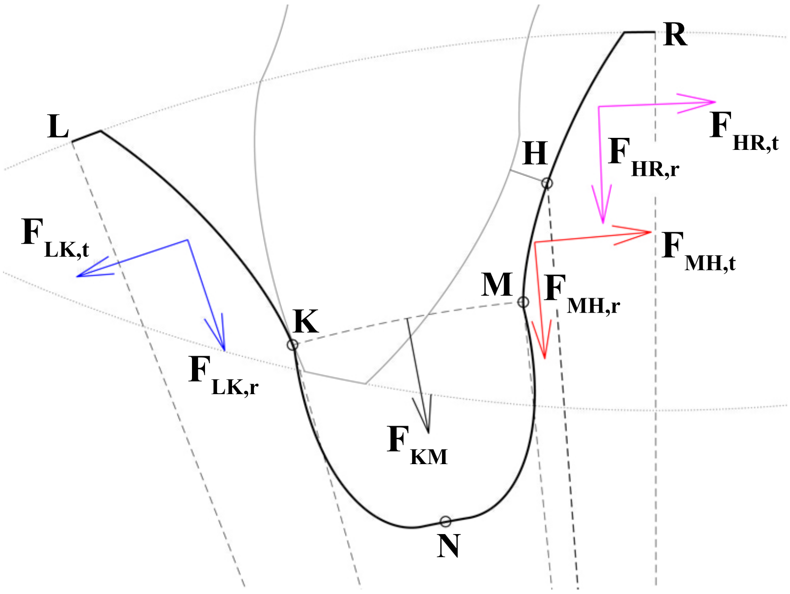

Figure 25: Detailed representation of the forces loading the tooth pocket surface along the line of approach.

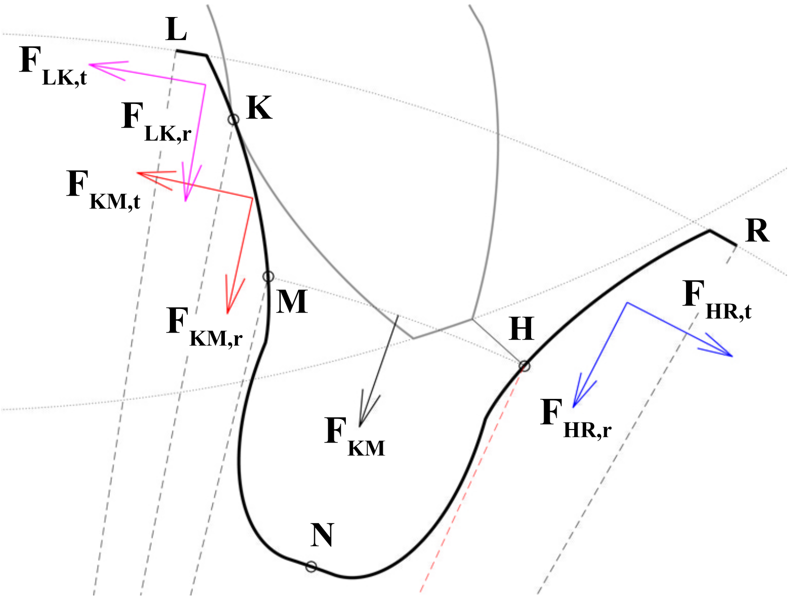

Figure 26: Detailed representation of the forces loading the tooth pocket surface along the line of recess.

divided in two components along the radial and tangential directions, namely $F_{LK,r}$ and $F_{LK,t}$ respectively(Figure 25), calculated with Eqns. 44 and 45:

$$|F_{LK,r}| = 2bP_{j-1}\sin\left(\frac{\vartheta_L - \vartheta_K}{2}\right) r_{ext} \tag{44}$$

$$|F_{LK,t}| = bP_{j-1}\sin\left(r_{ext} - r_K\right) \tag{45}$$

The presence of a non zero tangential component leads to the non-zero pressure torque T_{LK}, which can be calculated with the following Eqn. 46:

$$|T_{LK}| = |F_{LK,t}|\left(\frac{r_{ext} + r_K}{2}\right) \tag{46}$$

Force F_{LK} has now to be referred into the coordinates system of Figure 23 by using Eqns. 47 and 48:

$$F^x_{LK} = -|F_{LK,r}|\cos\left(\frac{\vartheta_L + \vartheta_K}{2}\right) - |F_{LK,t}|\sin\left(\frac{\vartheta_L + \vartheta_K}{2}\right) \tag{47}$$

$$F^y_{LK} = -|F_{LK,r}|\sin\left(\frac{\vartheta_L + \vartheta_K}{2}\right) + |F_{LK,t}|\cos\left(\frac{\vartheta_L + \vartheta_K}{2}\right) \tag{48}$$

A similar procedure can be applied to the right side of the tooth space, between points H and R (Figure 25); here, pressure P_j produces force F_{HR}, defined along the radial and tangential directions, and torque T_{HR}, which can be calculated with Eqns. 49, 50 and 51:

$$|F_{HR,r}| = 2bP_j\sin\left(\frac{\vartheta_H - \vartheta_R}{2}\right) r_{ext} \tag{49}$$

$$|F_{HR,t}| = bP_j\sin\left(r_{ext} - r_H\right) \tag{50}$$

$$|T_{HR}| = |F_{HR,t}|\left(\frac{r_{ext} + r_H}{2}\right) \tag{51}$$

As done regarding F_{LK}, force F_{HR} has to be referred into the coordinates system in Figure 23 applying Eqns. 52 and 53:

$$F^{x}_{HR} = -|F_{HR,r}|\cos\left(\frac{\vartheta_H + \vartheta_R}{2}\right) + |F_{HR,t}|\sin\left(\frac{\vartheta_H + \vartheta_R}{2}\right) \tag{52}$$

$$F^{y}_{HR} = -|F_{HR,r}|\sin\left(\frac{\vartheta_H + \vartheta_R}{2}\right) - |F_{HR,t}|\cos\left(\frac{\vartheta_H + \vartheta_R}{2}\right) \tag{53}$$

The middle part of the tooth pocket, which results to be bounded by points K and H, is subjected to pressure P_i; in this case, the pressure force is additionally subdivided into two forces, namely F_{KM} and F_{MH}. Force F_{KM} and torque T_{KM} are determined with Eqns. 54, 55 and 56:

$$|F_{KM,r}| = 2bP_i\sin\left(\frac{\vartheta_K - \vartheta_M}{2}\right)r_{ext} \tag{54}$$

$$|F_{KM,t}| = bP_i\sin\left(r_K - r_M\right) \tag{55}$$

$$|T_{KM}| = |F_{KM,t}|\left(\frac{r_K + r_M}{2}\right) \tag{56}$$

Concurrently, force F_{MH}, and the relative torque T_{MH}, are calculated with Eqns. 57, 58 and 59:

$$|F_{MH,r}| = 2bP_i\sin\left(\frac{\vartheta_M - \vartheta_H}{2}\right)r_{ext} \tag{57}$$

$$|F_{MH,t}| = bP_i\sin\left(r_H - r_M\right) \tag{58}$$

$$|T_{MH}| = |F_{MH,t}|\left(\frac{r_M + r_H}{2}\right) \tag{59}$$

Focusing the attention on Figure 25 and Figure 26, it can be noticed that the layout of the applied forces changes during the meshing evolution, due to a geometrical matter connected with the discretization adopted in the meshing zone. In particular, the scheme for the pressure force determination depends on the position of the contact point with respect to the line of action of the gears. When the meshing occurs along the line of approach (Figure 25), radius $r_K < r_H$ and $r_K = r_M$; therefore, $F_{KM,t}$ becomes zero, as well as torque T_{KM}, while $F_{MH,t}$ is applied on the right flank of the tooth space. On the opposite, when the meshing occurs along line of recess (Figure 26), radius $r_K > r_H$ and $r_H = r_M$; therefore, $F_{MH,t}$ becomes zero, as well as T_{MH}, while $F_{KM,t}$ is applied on the left flank of the tooth pocket. Force F_{KH}, defined as the sum of F_{KM} and F_{MH}, is calculated with Eqns. 60 and 61:

$$\begin{aligned} F^x_{KH} &= -|F_{KM,r}|\cos\left(\frac{\vartheta_K+\vartheta_M}{2}\right) - |F_{KM,t}|\sin\left(\frac{\vartheta_K+\vartheta_M}{2}\right) + \\ &\quad -|F_{MH,r}|\cos\left(\frac{\vartheta_M+\vartheta_H}{2}\right) + |F_{MH,t}|\sin\left(\frac{\vartheta_M+\vartheta_H}{2}\right) \end{aligned} \tag{60}$$

$$\begin{aligned} F^y_{KH} &= -|F_{KM,r}|\sin\left(\frac{\vartheta_K+\vartheta_M}{2}\right) + |F_{KM,t}|\cos\left(\frac{\vartheta_K+\vartheta_M}{2}\right) + \\ &\quad -|F_{MH,r}|\sin\left(\frac{\vartheta_M+\vartheta_H}{2}\right) - |F_{MH,t}|\cos\left(\frac{\vartheta_M+\vartheta_H}{2}\right) \end{aligned} \tag{61}$$

The total force $F_{tot,i}$ and the total torque $T_{tot,i}$ can be obtained from the sum of all the contributions estimated above:

$$F^x_{tot,i} = F^x_{LK} + F^x_{KH} + F^x_{HR} \tag{62}$$

$$F^y_{tot,i} = F^y_{LK} + F^y_{KH} + F^y_{HR} \tag{63}$$

$$T^z_{tot,i} = -|T_{HR}| - |T_{MH}| + |T_{LK}| + |T_{KM}| \tag{64}$$

Moreover, as observed regarding tooth spaces outside the meshing zone (Subsection 3.4.1), the tooth spaces geometry of spur gears leads to the absence of a pressure force component along axis z ($F^z_{tot,i} = 0$) and the two pressure torque components along axes x and y ($T^x_{tot,i} = 0$, $T^y_{tot,i} = 0$). By applying the calculus procedure from Eqn. 41 to Eqn. 64 to each tooth space, it is possible to determine the force and torque generated by the oil pressure inside each tooth space, which loads the gear center (by using Eqns. 42, 43 and 62-64). Thus, repeating such a procedure for each frame of calculus l, used to discretize a complete revolution, and summing, component by component, the pressure force and torque applied to each tooth space (by using Eqns. 65, 66 and 67), the total pressure force and torque applied to the gear center are obtained.

$$F^{x}(l) = \sum_{i=1}^{z_n} F_{tot,i}{}^{x}(l) \tag{65}$$

$$F^{y}(l) = \sum_{i=1}^{z_n} F_{tot,i}{}^{y}(l) \tag{66}$$

$$T^{z}(l) = \sum_{i=1}^{z_n} T_{tot,i}{}^{z}(l) \tag{67}$$

The present procedure can be straightforwardly applied to the driven gear; in this case if V_j is the reference control volume, then it is necessary to take into account the influence of control volumes V_i and V_{i+1}.

3.4.3 *Pressure load on the lateral sides of spur gears*

For the sake of completeness, it is worth considering that the presence of oil between the lateral sides of the gears and the bushes/thrustplates leads to the presence of a pressure distribution along the axial direction. The determination of such a load becomes of great importance in particular for a correct designing of the bushes and the sealing system with respect to the axial balance of the pump [55]. On the contrary, the present procedure has been specifically built up for the estimation of the variable pressure load acting along the facewidth of the gears, in order to estimate the pressure force and torque components, which have a significant influence on the dynamic behavior of the gears. In this context, the effects of the oil pressure loading the lateral sides of the gear have been neglected on the basis of geometrical considerations. On each side of a gear, in fact, the oil pressure gives a pressure force loading the gear along the axial direction. Moreover, the oil pressure also produces a pressure torque acting along a direction lying on the plane perpendicular to the gear axis of rotation. Nevertheless, since the two sides of a spur gear are symmetrical, if the relief groove milled on the casing and the clearances are symmetrical as well, the pressure force and torque acting on the two sides cancel each other out, reciprocally. On the other hand, if the relief grooves and the clearances are not symmetrical, the estimation of the pressure force and torque loading the gear sides strongly depends on the pump layout and the formulation cannot be generalized analytically, but it has to be performed numerically [55]. The first step is to estimate the pressure distribution on each side, then, with a numerical integration, calculate the pressure force, which can be supposed as axially oriented, and later detect its line of action with respect to the gear center. Finally, the pressure torque given by the pressure force components defined on the two gear sides can be determined.

3.4.4 *Evaluation of the methodology accuracy*

In the present section the results concerning the methodology presented in Subsections 3.4.1 and 3.4.2 are shown and discussed, comparing them with the results obtained applying previous methods described in [17, 16]. In order to carry out the assessment, the pressure distribution referring to a gear pump with main parameters reported in Tab. 6 has been calculated by adopting the mathematical model described in Section 3.2. In particular, the pressure distribution around the gearpair of the pump has been used as input data for the estimation of the pressure loads by using the proposed methodology and the method proposed in [17], namely Past Model 1 (PM1), and the method described in [16], namely Past Model 2 (PM2). These three methods are identified by a different way of modeling the pressure force and torque inside the meshing zone. In particular, in the PM1 the meshing phenomenon is not considered, therefore the pressure force is estimated by using Eqn. 41 along the entire revolution. Moreover, in the PM1 the pressure torque is calculated without considering the effects of the oil pressure between meshing teeth nor the one inside the trapping volume, but simply taking into account the pressure difference between inlet and outlet chambers. In the PM2, the effects produced during the meshing evolution on the pressure force are evaluated, but a different definition of the control volumes is used. The PM2 takes into

Table 6: Main characteristics of the pump adopted to assess the variable pressure loads estimation procedure.

Tooth number	17
Displacement	$8.1 * 10^{-7} m^3/rev$
Delivery pressure	$28 bar$
Working speed	$3020 rpm$

account the effects of the meshing phenomenon just when a double contact point exists and the trapping volume can be defined. When a single contact point exists, in the PM2 the pressure torque is estimated as in PM1.

Figure 27 shows the comparison between pressure force and torque on both driving and driven gear, obtained by applying the new methodology (from Eqn. 41 to Eqn. 67), namely current methodology CM, and the PM1 for the pump reported in Tab. 6. Each pressure force component is normalized by applying Eqn. 68:

$$F^* = \frac{F_p}{2 r_{rext} P_{out} b} \tag{68}$$

Concurrently, each pressure torque component is normalized applying Eqn. 69:

$$T^* = \frac{T_p}{b P_{out} \frac{r_{ext}^2 - r_{root}^2}{2}} \tag{69}$$

As already discussed, the PM1 does not take into account the meshing phenomena, which results in a low level of agreement between these two methods. In particular, the estimation of the pressure torque on the driving gear appears to give completely different results (Figure 27.c), while there is, in general, a good accordance regarding the estimation of the pressure torque applied on the driven gear (Figure 27.f). The lack of agreement in the estimation of the pressure torque is due to the different approach: in the CM the pressure torque directly derives from the estimation of the pressure force applied along the tangential direction whilst in the PM1 the pressure torque is evaluated analyzing the meshing phenomenon geometrically.

In order to better understand why the estimation of the pressure force by using PM1 method gives so different results, it is possible to focus the atten-

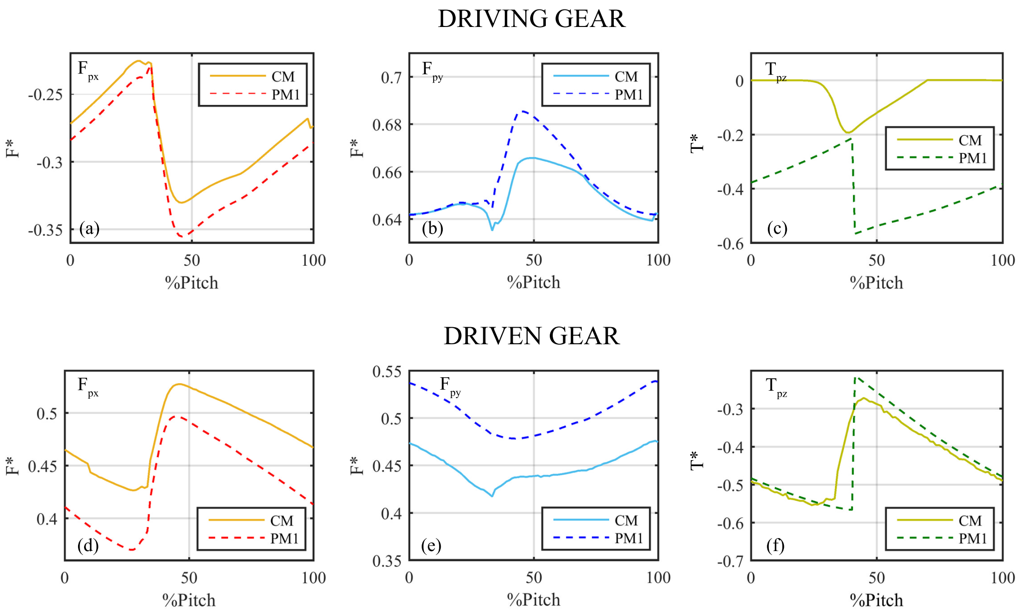

Figure 27: Comparison between pressure force and torque along the angular pitch for both driving and driven gear, calculated with the PM1 and the CM.

tion, as an example, on the pressure force transmitted along the axis y by the tooth space defined by volume V_j (belonging to a driven gear) during a complete revolution. In Figure 28 the course of such a pressure force component during a complete revolution calculated by using the CM and by using the PM1 is shown, together with the pressure evolution inside the control volumes used for their determination. As expected, the two forces coincide for the entire revolution, except for the meshing interval, in which the PM1 does not take into account the effect produced by two phenomena: (i) the slight difference between the pressure evolution in control volumes V_j and V_i, and (ii) the pressure drop in control volume V_{i+1} that occurs an angular pitch before the pressure drop in V_i. This latter phenomenon strongly affects the pressure force effectively transmitted to the gear axis and, therefore, it cannot be neglected. The phenomenon (ii), in particular, is taken into account in the calculus procedure defined by PM2, which has been demonstrated to give more accurate results with respect to PM1 in the elasto-dynamic analysis of gear pumps [16].

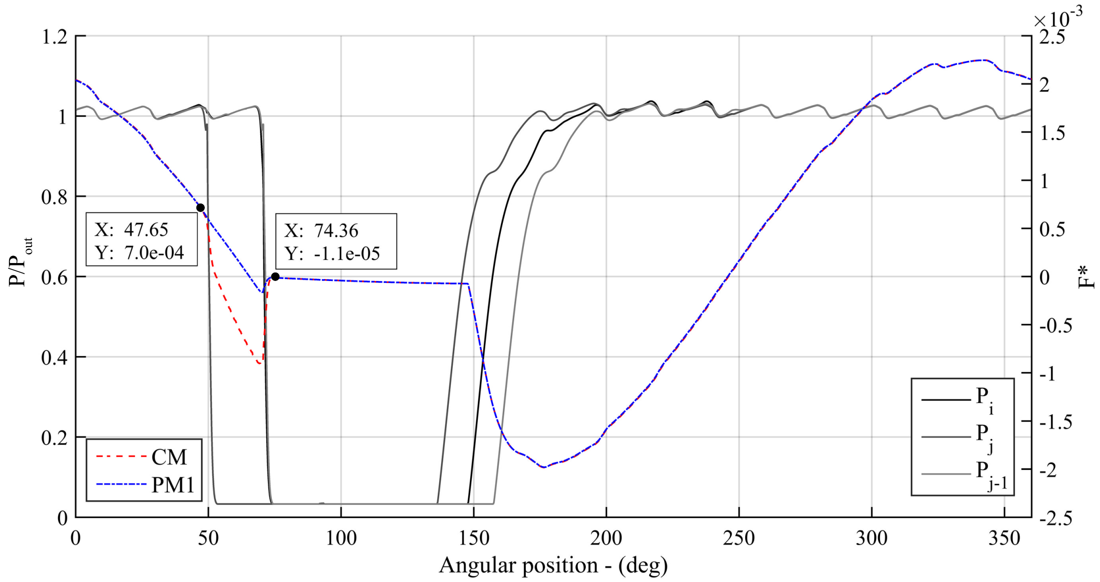

Figure 28: F_Y transmitted by a single tooth space V_j during a complete revolution estimated by using the CM and by using the PM1; pressure evolution in the tooth spaces used for the force estimation. P_{out} refers to the delivery pressure in Tab. 6.

Figure 29 shows the same comparison between the CM and the PM2 applied to the pump in Tab. 6. As it can be noticed, the two methods provide an almost coincident estimation of the pressure force transmitted along x direction, while a major level of discordance is observed in the estimation of the pressure force transmitted along y direction. These light discrepancies occur because of the procedure defined in PM2, which does not take into account the phenomenon (i). The oil pressure inside the tooth spaces referred to two meshing teeth, as observed in Figure 29, is almost equal during the meshing evolution. Nevertheless, when these tooth spaces start facing to the inlet chamber, the pressure drop in both control volumes determines an increase of the pressure difference between them and, therefore, a light difference in the pressure force estimated by the two models occurs.

Regarding the pressure torque, it is possible to observe that similar results are obtained only till the 35% of the angular pitch (Figure 29.c and Figure 29.f); the remaining 65% is characterized by a higher level of discordance, especially for the pressure torque applied on the driving gear. The reason of